Phosphoproteomics Analysis Identifies Novel Candidate Substrates of the Nonreceptor Tyrosine Kinase, *Src-r*elated Kinase Lacking C-terminal Regulatory Tyrosine and N-terminal *My*ristoylation *S*ites (SRMS)*[S]

Raghuveera Kumar Goel‡, Marta Paczkowska§, Jüri Reimand§¶, Scott Napper‡‖, and Kiven Erique Lukong‡**

SRMS (*S*rc-related kinase lacking C-terminal *r*egulatory tyrosine and N-terminal *m*yristoylation sites), also known as PTK 70 (Protein tyrosine kinase 70), is a non-receptor tyrosine kinase that belongs to the BRK family of kinases (BFKs). To date less is known about the cellular role of SRMS primarily because of the unidentified substrates or signaling intermediates regulated by the kinase. In this study, we used phosphotyrosine antibody-based immunoaffinity purification in large-scale label-free quantitative phosphoproteomics to identify novel candidate substrates of SRMS. Our analyses led to the identification of 1258 tyrosine-phosphorylated peptides which mapped to 663 phosphoproteins, exclusively from SRMS-expressing cells. DOK1, a previously characterized SRMS substrate, was also identified in our analyses. Functional enrichment analyses revealed that the candidate SRMS substrates were enriched in various biological processes including protein ubiquitination, mitotic cell cycle, energy metabolism and RNA processing, as well as Wnt and TNF signaling. Analyses of the sequence surrounding the phosphosites in these proteins revealed novel candidate SRMS consensus substrate motifs. We utilized customized high-throughput peptide arrays to validate a subset of the candidate SRMS substrates identified in our MS-based analyses. Finally, we independently validated Vimentin and Sam68, as bona fide SRMS substrates through *in vitro* and *in vivo* assays. Overall, our study identified a number of novel and biologically relevant SRMS candidate substrates, which suggests the involvement of the kinase in a vast array of unexplored cellular functions. *Molecular & Cellular Proteomics 17: 925–947, 2018. DOI: 10.1074/mcp.RA118.000643.*

Tyrosine kinases are key enzymes that regulate various cellular and physiological functions by phosphorylating tyrosine residues on substrate proteins (1). The human genome project identified 90 tyrosine kinases of which 58 are receptor type and 32 are non-receptor type tyrosine kinases (2). *S*rc-related kinase lacking C-terminal *r*egulatory tyrosine and N-terminal *m*yristoylation *s*ites (SRMS)[1] or PTK70, is a non-receptor tyrosine kinase that belongs to the BRK family kinases and is evolutionarily related to c-Src (3, 4). The gene encoding SRMS was first discovered in 1994 in a screen for novel genes regulating neural precursor cell differentiation (5). The gene maps to the chromosomal locus 20q 13.33 and is positioned adjacent to BRK on the same locus (3, 6).

From the ‡Department of Biochemistry, College of Medicine, 107 Wiggins Road, University of Saskatchewan, Saskatoon S7N 5E5, Saskatchewan, Canada; §Computational Biology Program, Ontario Institute for Cancer Research, 661 University Ave Suite 510, Toronto M5G 0A3, Ontario, Canada; ¶Department of Medical Biophysics, University of Toronto, 101 College Street Suite 15–701, Toronto M5G 1L7, Ontario, Canada; ‖Vaccine and Infectious Disease Organization - International Vaccine Centre (VIDO-InterVac), 120 Veterinary Road, University of Saskatchewan, Saskatoon S7N 5E3, Saskatchewan, Canada

Received January 30, 2018

Published, MCP Papers in Press, February 28, 2018, DOI 10.1074/mcp.RA118.000643

Author contributions: R.K.G. and K.E.L. designed research; R.K.G. performed research; R.K.G., M.P., J.R., and S.N. analyzed data; R.K.G. and K.E.L. wrote the paper; J.R. critical review of the manuscript.

[1] The abbreviations used are: SRMS, Src-related kinase lacking C-terminal regulatory tyrosine and N-terminal myristoylation sites; PTK 70, Protein tyrosine kinase 70; BRK, Breast tumor kinase; FRK, Fyn-related kinase; Sam68, Src associated substrate during mitosis of 68kDa; BFK, BRK family kinase; SH3, Src-homology domain 3; SH2, Src-homology domain 2; SFK, Src family kinases (SFKs); PTB, Phosphotyrosine-binding domain; FDR, F*alse discovery rate*; GNL3L, G Protein Nucleolar 3 Like; CKAP2, Cytoskeleton Associated Protein 2; HNRNPM, Heterogeneous Nuclear Ribonucleoprotein M; EIF4A3/1, Eukaryotic initiation factor 4A-III; KRT18, keratin 18; UMPS, Uridine Monophosphate Synthetase; MCM7, Minichromosome Maintenance Complex Component 7; GRB10, Growth Factor Receptor Bound Protein 10; KHDRBS1, KH domain-containing, RNA-binding, signal transduction-associated protein 1; EGF, Epidermal Growth Factor; EGFR, Epidermal Growth Factor Receptor.

The *SRMS* gene encodes a 54 kDa protein spanning 488 amino acids (6). Like other members of the BRK family, namely BRK/PTK6 (Breast tumor kinase/Protein tyrosine kinase 6) and FRK/PTK5 (Fyn-related kinase/Protein tyrosine kinase 5) as well as members of Src family kinases (SFKs), the SRMS protein is composed of a Src-homology 3 (SH3) domain, a Src-homology 2 domain (SH2) and a kinase domain (6). Both, SH3 and SH2 domains are known to be involved in intra- and intermolecular interactions (7–10). Although the SH3 domain binds to poly-proline motifs, the SH2 domains binds to phosphotyrosine-containing motifs (7–10). A previous study from our group characterized DOK1 as a SRMS substrate and reported that the SRMS SH3 and SH2 domains associate with DOK1 *in vitro* (6). We further reported that the presence of the 50-amino-acid-long N-terminal region of SRMS is essential for its enzymatic activity and consequently for the phosphorylation of DOK1 (6). As with other kinases, two key conserved residues, namely the ATP-contacting lysine, K258 and the primary autophosphorylation site in the activation loop, Y380, were also shown to be essential for the enzymatic activation of SRMS (6). A recent study identified BRK as another SRMS substrate and interestingly SRMS was shown to directly phosphorylate the C-terminal regulatory tyrosine residue (Y447) in BRK (11). This identified a biochemical basis for SRMS as a potential regulator of BRK enzymatic activity, although further investigations are pending.

Several studies have characterized the biochemical and cellular roles of BRK and FRK and have reported the involvement of these kinases primarily in the regulation of cell growth via interaction with and/or phosphorylation of key cellular proteins (3, 4). Although several binding partners and substrates have been identified and characterized for BRK and FRK (3, 4), only two substrates (DOK1 and BRK) have been identified for SRMS so far (6, 11). Consequently, SRMS biology is the least understood of the BRK family kinases. A limited number of investigations pursued in the past have provided clues into the potential functional significance of the kinase in mammalian cells. For instance, Kohmura *et al.* noted that SRMS expression was temporally and spatially altered in the mouse brain during the embryonic developmental stages, suggesting a potential involvement of SRMS in neural cell differentiation (5). Another study by Kawachi *et al.* reported that SRMS was expressed in the normal epidermal and keratinocyte cells and may be involved in keratinocyte differentiation (12). Furthermore, in these studies SRMS expression was detected in various other murine organs such as the lung, liver, spleen, ovary, kidney, intestines and testis (5, 12).

Though nonreceptor tyrosine kinases constitute only about 6% of the total kinases encoded by the human genome (2), these kinases play physiologically significant roles linked to mammalian growth and development (13, 14). Like serine/threonine kinases, tyrosine kinases phosphorylate various substrate proteins to regulate specific intracellular signaling pathways which ultimately elicit specific cellular and physiological functions (15). The catalytic activity of tyrosine kinases is highly regulated in eukaryotic cells and involve biochemically distinct mechanisms of autoregulation (16–18). Furthermore, these kinases are known to exhibit distinct biochemical substrate-motif specificities which are believed to impart specificity to the cellular functions regulated by these kinases (19–21). To date, high-throughput phosphoproteomics approaches have been applied to identify the cellular substrates of very few non-receptor tyrosine kinases (22–24). Thus, key questions remain unanswered regarding the cellular roles and biochemical specificities of other non-receptor tyrosine kinases. We previously noted that the expression of wild type SRMS in HEK293 cells induced the tyrosine phosphorylation of several endogenous proteins (6). These proteins represent the potential cellular substrates of SRMS and are largely unidentified. The identity of these candidate cellular substrates of SRMS would be essential for a better understanding of the role of SRMS in mammalian cell biology.

Mass spectrometry-based interrogation of the cellular phosphoproteome has afforded high-throughput and robust identification of various serine/threonine and tyrosine kinase substrates and associated signaling intermediates (22–27). Over the years, the technology has been used to precisely quantify multiple phosphorylation events occurring dynamically in the cellular phosphoproteome (28, 29).

In the present study, we quantitatively probed the tyrosine-phosphoproteome of HEK293 cells upon the exogenous introduction of wild type SRMS and identified 663 candidate substrates of the kinase. Motif analyses revealed novel SRMS substrate consensus sequences among the candidate SRMS substrates. We used customized high-throughput peptide arrays and validated a subset of the candidate SRMS substrates. We finally independently validated Vimentin and Sam68, as bona fide SRMS substrates via immunoprecipitation analyses as well as direct *in vitro* kinase assays.

EXPERIMENTAL PROCEDURE

Cell Lines, Cell Culture, and Transfections—Human embryonic kidney (HEK) 293, HeLa and MDA-MB 231 cells were cultured at 37 °C in DMEM High glucose media (SH30243.01, Hyclone, Pittsburgh, PA) supplemented with 10% FBS. All transfections were performed using 1% Polyethyleneimine (PEI) solution prepared from linear polyethyleneimine (#23966, Polysciences Inc., Warrington, PA). For plasmid transfections, HEK293 or HeLa cells were seeded in 6-well plates or 10 cm plates and cultured to approx. 80% confluency. 2.5 μg (6-well plates) or 10 μg (10 cm plates) DNA was dissolved in 107.5 μl (6-well plate) or 430 μl (10 cm plate) of 0.15 M NaCl via gentle vortexing for 10 s. Next, 15 μl (6-well plate) or 60 μl (10 cm plate) of 1% PEI was added to this mix, gently vortexed for 10 s and incubated at room temperature for 10 mins. The DNA-PEI mix was then dispensed dropwise into the culture dishes, supplemented with fresh media. The dishes were gently swirled and returned to the tissue culture incubator for overnight incubation. SRMS or scramble siRNAs were transfected using the RNAiMAX transfection reagent (Thermo Fisher Scientific, Waltham, MA) according to the manufacturer's instructions. For stimulating cells with EGF, MDA-MB 231 cells were serum starved

overnight and treated with 100 ng/ml EGF for various times and lysed for use as total cell lysates or for immunoprecipitation.

Plasmids and siRNA—The pEGFP-C1 plasmid was purchased from Clontech, Mountain View, CA. Plasmids encoding GFP-tagged wild type SRMS, ΔN-SRMS (N-terminal deletion mutant) or SRMS K258M (kinase-dead mutant), constructed using the pEGFP-C1 backbone vector, have been previously described (6). EGFP-Vimentin-7 (referred to as GFP-Vimentin herewith) was a gift from Michael Davidson (Addgene plasmid # 56439). The Vimentin cDNA sequence was amplified from the EGFP-Vimentin construct using the primers: 5′-AAAAAAAGCTTCGATGTCCACCAGGTCCGTGTCC-3′ and 5′-AAAAAGGATCCTCATTCAAGGTCATCGTGATGCTG-3′ and cloned into the HindIII and BamHI restriction sites in the pmCherry-C1 vector (Clontech). Vectors encoding Myc-Sam68 and GFP-Sam68 have been described before (30). N-terminal Flag-tagged wild type SRMS or SRMS K258M cDNA sequences were cloned into the Not1 and BamH1 restriction sites of the pQCXIH vector (Clontech) using the primer pair: 5′-AAAAGCGGCCGCGCCACCATG*GACTACAAAGACG-ATGACGACAAG*GAGCCGTTCCTCAGGA-3′ (Flag-tag nucleotide sequence underlined) and 5′-AAAAGGATCCTCAGGGGTGGCATCTG-TGGATGGCGTG-3′. An alternate forward primer was paired with the same reverse primer to generate an untagged wild type SRMS construct using the pQCXIH vector backbone: 5′-AAAAGCGGCCG-CATGGAGCCGTTCCTCAGGA-3′. cDNA encoding the SRMS kinase was amplified using the primers: 5′-AAAAAGGATCCATGCCCCAGA-AGGCCCCGAGG-3′ and 5′-AAAAACTCGAGTCAGGGGTGGCATC-TGTG-3′ and cloned into the BamH1 and Xho1 restriction sites in-frame with the GST sequence of the pGEX-6p1 vector. To generate the GST-Vimentin construct, the Vimentin cDNA sequence was amplified using the primers: 5′-AAAAAGGATCCATGTCCACCAGGTCC-GTG-3′ and 5′-AAAAAGTCGACTCATTCAAGGTCATCGTGATGCT-G-3′ and cloned into the BamHI and SalI restriction sites of the pGEX-6P1 VECTOR. Similarly, cDNA sequence encoding Sam68 was amplified using primers: 5′-AAAAAGTCGACTCATGCAGCGCCGGG-ACGACCCCGCCGCG-3′ and 5′-AAAAAGCGGCCGCTCAATAACG-TCCATATGGGTG-3′ and cloned into the SalI and NotI sites of the pGEX-6p1 vector. SRMS siRNA (sc-63066) and scramble (control) siRNA (sc-37007) were purchased from Santa Cruz Biotechnologies. The SRMS siRNA is a pool of 2 duplexed siRNAs, namely, Sc-63066A (sense- CUUGCGCUCUAUGACUUCAtt and antisense- UGAAGU-CAUAGAGCGCAAGtt) and Sc-63066B (sense- GCGAUCAAGGU-CAUCAAGUtt and antisense- ACUUGAUGACCUUGAUCGCtt).

Antibodies—Phosphotyrosine antibodies, 4G10 (#05–321) and pTyr 1000 (#8954) were procured from EMD Millipore, Danvers, MA and Cell Signaling Technologies, Danvers, MA, respectively. Flag antibodies (#MA1–91878) were purchased from Thermo-Scientific. The well characterized Sam68 antibody, AD1, has been described before (31) and was used for immunoprecipitation experiments. All other primary antibodies were purchased from Santa Cruz Biotechnologies (Santa Cruz, Dallas, Texas). These include antibodies against GFP (#sc-101525), GST (#sc-459), SRMS (#sc-374524), Myc (#sc-40), Sam68 (#sc-1238) and β-actin (#sc-47778). Secondary antibodies for Western blotting analyses namely, goat anti-rabbit (IR Dye-680RD IgG, #926–68071) and goat anti-mouse (IR Dye-800CW IgG, #926–32210), were purchased from Li-Cor Odyssey, Lincoln, NE. Secondary goat anti-mouse IgG-Texas red (#sc-2781) antibodies were purchased from Santa Cruz Biotechnologies (Santa Cruz).

Experimental Design and Statistical Rationale—We adopted a label-free phosphoproteomics strategy and generated samples for LC-MS/MS accordingly. HEK293 cells were cultured to nearly 85% confluency in a total of 24 × 10 cm dishes. 12 × 10 cm dishes were transfected with plasmids encoding either GFP-SRMS wild type (SRMS-WT) or GFP alone as control (sample size per experiment, $n = 2$). Twenty-four hour post-transfection, transfections efficiencies were determined via fluorescence microscopy (Olympus 1 × 51) and estimated to be over 90% in both conditions. The experiment was performed in two biological replicates. Both replicates were analyzed via LC-MS/MS. Peptide and protein searches were performed using the Andromeda search engine (integrated in MaxQuant, version 1.5.3.17) at an FDR threshold of 1%. Statistical analysis of the identified phosphopeptides was performed using the Perseus platform (version 1.5.0.15). Precursor ion intensities corresponding to tyrosine-phosphorylated peptides were transformed to logarithmic scale (log2). Phosphopeptides that were identified in only one replicate were discarded. Statistical significance was computed using the two-sample student's *t* test in the Perseus platform and phosphopeptides filtered at a threshold *p* value of 0.05. The resulting statistically significant peptides were segregated as either unique to GFP alone, GFP-SRMS-WT or both.

Protein Digestion and Purification of Tryptic Peptides—Twenty-four hour post-transfection, the cells were lysed in lysis buffer comprising 9 M Urea and 20 mM HEPES pH 8.0. The respective lysates were pooled in sterile 50 ml conical tubes and sonicated four times with 10-s bursts using the Virsonic 100 ultrasonic cell disruptor (Boston Laboratory Equipment, Woburn, MA). These were then centrifuged at 15,000 r.c.f. and the supernatants transferred to sterile 50 ml conical tubes. Total protein concentration was determined via Bradford's assay (#500–0006, Bio-Rad, Hercules, CA). 12 mg total lysate protein, each from GFP and GFP-wild type SRMS-expressing cells, was taken for further processing. Proteins were reduced with Dithiothreitol (DTT) (#D9779, Sigma-Aldrich, St. Louis, MO) and alkylated with iodoacetamide (#I6125, Sigma-Aldrich). The reduced and alkylated proteins were diluted 4-fold with 20 mM HEPES pH 8.0 and digested with trypsin (#LS003740, Worthington Biochemical Corporation, Lakewood, NJ) at a 1:100 enzyme to protein ratio (w/w) overnight at 37 °C. Crude tryptic digests were purified via reversed-phase (hydrophobic) solid-phase extraction using Sep-Pak cartridges (#WAT051910, Waters Corporation, Milford, MA). Briefly, the tryptic digests were loaded on the purification cartridges, washed with 0.1% trifluoroacetic acid (TFA) (#28903, Thermo-Scientific) and eluted with 0.1% TFA and 40% acetonitrile (#51101, Thermo-Scientific). The purified tryptic peptides were then lyophilized and used toward enrichment of phosphotyrosine peptides.

Enrichment of Phosphotyrosine Peptides—The enrichment of tyrosine-phosphorylated peptides was performed using the PTMScan p-Tyr 1000 phosphotyrosine enrichment kit (#8803, Cell Signaling Technologies). Briefly, the lyophilized peptide samples were re-suspended in 1x Immunoaffinity purification (IAP) buffer provided in the kit. The diluted peptides were then centrifuged at 10,000 r.c.f. for 5 min at 4 °C. The clear supernatant was retained. The pTyr-1000 antibody-bead conjugates were then washed with 1x PBS and incubated with the peptide mix overnight at 4 °C on a gyrorotator. The following day, the immunoprecipitates were serially washed with LC-MS-grade water (#51140, Thermo-Fisher Scientific) and 1x PBS. The immunoprecipitated peptides were then eluted with 0.1% TFA at room temperature. The eluted peptides were desalted using the Empore C18 solid phase extraction plate (#66875, Sigma-Aldrich) as per the manufacturer's protocol.

Reversed-phase Chromatography and Mass Spectrometry—Samples were analyzed by nano UPLC-MS/MS with a Proxeon EASY-nLC 1000 system interfaced to a Thermo-Fisher Q Exactive HF mass spectrometer (Sample analyses performed by MSBioworks Inc., Ann Arbor, Michigan). Peptides were loaded on a trapping column and eluted over a 75 μm × 25 cm analytical column (Thermo-Fisher Scientific) at 300 nL/min using a 2 h reversed-phase gradient. Both columns were packed with PepMap C18, 3 μm resin (Thermo-Fisher Scientific). Mobile phases A and B consisted of 0.1% formic acid in water and 0.1% formic acid in 90% acetonitrile, respectively. Pep-

tides were eluted from the column at 300 nL/min using the following linear gradient: from 2 to 25% B in 100 min, from 25 to 50% B in 110 min, from 50 to 90% B in 112 min, from 90 to 2% B in 113 min and held at 2% B for an additional 7 min. The spray voltage was 2.2 kV. The mass spectrometer was operated in the Data- Dependent mode with the Orbitrap operating at 60,000 FWHM and 17,500 FWHM for MS and MS/MS respectively. Full scans were acquired at a resolution of 60,000 FWHM with a maximum injection time of 120 ms in the Orbitrap analyzer. The fifteen most abundant ions, with charge states $\geq$2, were selected for fragmentation by HCD (MS/MS) and analyzed at a resolution of 17,500 FWHM with a maximum injection time of 60ms.

Data Processing and Analysis—All acquired MS/MS spectra were searched against the Uniprot human complete proteome FASTA database v.02/2013 (81,213 entries) using the MaxQuant software (Version 1.5.3.17) that integrates the Andromeda search engine. Label-free quantitation of the data was performed using MaxQuant. Enzyme specificity was set to trypsin and up to two missed cleavages were allowed. Cysteine carbamidomethylation was specified as fixed modification whereas serine, threonine and tyrosine phosphorylation were specified as variable modifications. Peptide precursor ions were searched with a maximum mass deviation of 6 ppm and fragment ions with a maximum mass deviation of 20 ppm. Peptide and protein identifications were filtered at 1% FDR using the target-decoy database search strategy (32). Proteins that could not be differentiated based on MS/MS spectra alone were grouped to protein groups (default MaxQuant settings). Following the principle of parsimony, each protein group was considered a single identified protein for further data analyses because sufficient evidence was unavailable to distinguish between proteins from the same protein group. A threshold Andromeda score of 40 and a threshold delta score of 8 was applied to the identified phosphopeptides, in accordance with parameters described previously (33–35). Pearsons's correlation coefficients were determined in R using $\log_2$ transformed phosphopeptide intensities, as described before (36, 37). The MaxQuant file output designated "Phospho(STY)sites" used for further analysis using the Perseus software (Version 1.5.0.15). Potential contaminants and reverse hits were filtered. The resulting list of modified peptides was further filtered at the level of phospho-site localization using a localization probability threshold of 0.75 to derive all class I phospho-sites, as described previously (35). For downstream analyses, all peptides with modifications other than phosphotyrosine (pTyr) were discarded. Annotated spectra for class I phosphosites identified as statistically significant, are provided in the supplementary material.

Accession Number—The mass spectrometry proteomics data (including the files for viewing the annotated spectra) have been deposited to the ProteomeXchange Consortium (38) via the PRIDE (39) partner repository with the dataset identifier PXD006809. The data can be accessed on https://www.ebi.ac.uk/pride/archive/login using the following reviewer account details:

Username: reviewer22933@ebi.ac.uk

Password: xu7lPykO

Expression of Recombinant GST-fused Proteins—All recombinant GST-fused proteins (GST-SRMS kinase, GST-Vimentin and GST-Sam68) were expressed in the *E. coli* Rosetta™ (DE3) strain (#7094, EMD Millipore). Briefly, the Rosetta strains transformed with the respective plasmids, were cultured in Terrific broth (BP-2468–2, Fisher Scientific, Hampton, NH) until $Abs._{600} \sim 0.8$. The expression of the GST-fused proteins was induced with 0.5 mM IPTG at 37 °C for 3 h. Bacteria were then harvested via centrifugation at 7000 r.c.f. and the pellets lysed in freshly prepared lysis buffer (50 mM Tris.Cl pH 7.4, 300 mM NaCl, 0.5% TritonX-100 and protease inhibitors). The recombinant proteins were purified from the crude lysates by incubating with GST resin (70541, EMD Millipore) overnight at 4 °C. The beads were washed several times with lysis buffer and GST-fusion proteins eluted with 10 mM glutathione (G4251, Sigma), 50 mM Tris.Cl pH 7.4 and 1 mM DTT.

Immunoprecipitation and In Vitro Kinase Assays—For immunoprecipitation assays, cells were lysed in buffer comprising 50 mM Tris.Cl, 150 mM NaCl, 10% TritonX-100, 0.6 μg/ml Aprotinin, 1 mM PMSF, 1 mM Na_3VO_4, incubated on ice for 30 min and centrifuged at 20,000 r.c.f. at 4 °C for 10 min. The supernatant was retained and the 4 μg primary antibody was added to the clarified lysates. The lysates were incubated with the antibody overnight at 4 °C on a gyrorotator. The following day, 40 μl of the antibody isotype-matched protein A or protein G beads were added to the lysates and incubated on the gyrorotator at 4 °C for 1 h. The beads were centrifuged at 3500 r.c.f. for 1 min, washed 2 times with lysis buffer and immunoprecipitates eluted with the addition of 30 μl 2× sample buffer concentrate (#S3401–10VL, Sigma-Aldrich). The samples were boiled at 100 °C for 5 min and resolved via SDS-PAGE.

For *in vitro* kinase assays, GST-Sam68 or GST-Vimentin, were incubated with GST-SRMS kinase in *in vitro* kinase buffer (250 μM unlabeled ATP, 5 mM MOPS, pH 7. 2, 2.5 mM β-glycerol-phosphate, 4 mM MgC12, 2.5 mM MnC12, 1 mM EGTA, 0.4 mM EDTA and 0.5 mM DTT) for 30 min at 30 °C. The *in vitro* kinase reactions were quenched by the addition of 2× sample buffer, boiled, and loaded on SDS-PAGE gels.

Confocal Microscopy Analyses—Cells were seeded on glass coverslips in 6-well cell culture plates, transfected and cultured overnight. The following day, the culture media was aspirated and the cells fixed with 3% paraformaldehyde (PFA) for 10 min. The fixed cells were permeabilized with 0.5% Triton X-100 and either directly mounted on glass slides using mounting media supplemented with DAPI (4′,6-diamidino-2-phenylindole) (#P36960, Thermo-Fisher Scientific) or incubated with the appropriate primary antibody and secondary antibodies prior to mounting. Fluorescence imaging was performed using the Zeiss confocal laser scanning microscope (LSM) system (LSM-700, Carl Zeiss). The LSM 700 system was equipped with the inverted Axio Observer.Z1 SP microscope. All images were acquired using the Zen 2012 SP1 (64-bit, black edition) software (Carl Zeiss). Fluorescence from the EGFP protein and Texas-red (sulforhodamine 101 acid chloride)-conjugated antibodies was excited, respectively, using the 488 nm and 555 nm lasers (4× Pigtailed laser with single-mode fibers, Carl Zeiss). Fluorescence from the DAPI dye was excited using the 405 nm laser (4× Pigtailed laser with single-mode fibers, Carl Zeiss). All images were acquired at 40× magnification (40× oil-immersion objective) with a resolution of 1024 × 1024 pixels and a pixel-bit depth of 16 bits. Where necessary, images were acquired using at least two averaging scans to enhance the signal-to-noise ratio. Colocalization between two proteins, with different fluorescence emissions, was assessed by employing the z-stack function of the LSM 700 confocal microscope. The number of z-stack scans and the spatial interval between each scan was appropriately defined to scan the region of interest.

Peptide Array Analyses—Customized peptide microarrays (PepStar™) comprising 102 peptides were manufactured by JPT peptide technologies GmbH (Germany). The peptides were immobilized on modified glass slides at a concentration of 100 fmol/mm^2 with a maximum diametrical spot size of 150 μm on the glass surface. Each peptide was printed on the array in 9 replicates. The array peptides and the corresponding phospho-sites are listed in supplemental Table S6. HEK293 cells, cultured in four 10 cm dishes, were transfected with vectors encoding either GFP-SRMS K258M or GFP-SRMS wild type. Twenty-four hours post-transfection, the cells were harvested and lysed in lysis buffer (20 mM tris-HCl (pH 7.5), 150 mM NaCl, 1 mM EDTA, 1 mM ethylene glycol tetraacetic acid (EGTA), 1% Triton, 2.5 mM sodium pyrophosphate, 1 mM Na_3VO_4, 1 mM NaF, leupeptin (1

μg/ml), aprotinin (1 g/ml) and 1 mM phenylmethylsulphonyl fluoride (PMSF)). The lysates were incubated on ice for 10 min and centrifuged in a microcentrifuge at maximum speed for 10 min at 4 °C. Total protein concentration in the lysates was determined (Pierce BCA protein assay kit, Thermo Fisher Scientific) and normalized using the appropriate volume of lysis buffer. An 80 μl aliquot of the clarified supernatant was mixed with 10 μl of the activation mix (50% glycerol, 500 μM ATP, 60 mM $MgCl_2$, 0.05% v/v Brij-35, and bovine serum albumin (BSA, 0.25 mg/ml)) and incubated on the peptide arrays for 2 h at 37 °C in a humidity chamber. The slides were then washed once in PBS-Triton (1% TritonX-100 in 1x PBS) and then stained with a phosphoprotein staining solution (PRO-Q, Diamond Phosphoprotein Stain, Invitrogen, Burlington, Canada) with agitation for 1 h. The arrays were then washed three times with the de-staining solution (20% acetonitrile (EMD Biosciences, Billerica, MA) and 50 mM sodium acetate (Sigma, Oakville, Canada) at pH 4.0) for 10 min each. The de-staining solution was replaced between each wash. The peptide arrays were then washed once with distilled water and scanned on the GENEPIX professional 4200A microarray scanner (MDS Analytical Technologies) at 532 to 560 nm with a 580 nm filter to detect dye fluorescence. Phosphopeptide signals were collected using the GENEPIX 6.0 software (MDS). Data processing, including signal normalization and relative fold-change differences in phosphorylation intensity associated with each peptide, was performed using the PIIKA2 platform (40) (http://saphire.usask.ca/saphire/piika/).

Functional Gene Enrichment Analyses—Pathway enrichment analysis of the putative SRMS substrates was performed using the g:Profiler software (Ver. r1741_e90_eg37) (41). A background set of 13,505 unique phosphorylated proteins, comprising phosphorylated proteins identified in our MS analyses as well as those derived from proteomics datasets available with PhosphositePlus.org (42), was used to compute the enrichment of statistically significant cellular pathways or processes. We retrieved gene sets corresponding to biological processes from Gene Ontology with statistical enrichment among input proteins (FDR$<$0.05 according to the internal multiple testing correction method of g:Profiler). Gene sets were filtered by size (minimum size of functional gene set 10, maximum size of functional gene set 500, at least 3 common genes of pathway and input protein list). We included high-confidence annotations of biological processes and excluded genes with only electronic annotations in GO (Inferred from Electronic Annotations, IEA). The resulting enriched pathways were visualized with the Enrichment Map software (43) in Cytoscape (Ver. 3.0). We used a combined overlap and Jaccard coefficient of 0.75 for network granularity and manually annotated the resulting subnetworks of pathways for associated biological themes.

RESULTS

SRMS Induces Kinase-dependent Tyrosine Phosphorylation of Cellular Proteins—We previously reported wild type SRMS as a catalytically active tyrosine kinase whose enzymatic activity is primarily regulated by the first 50 amino acids in the N-terminal region of the protein (6). We observed that the exogenous expression of wild type SRMS and not ΔN-SRMS (N-terminal deletion) or SRMS-K258M mutants resulted in increased tyrosine phosphorylation of cellular proteins (6). We confirmed this finding by ectopically expressing GFP-tagged constructs encoding either wild type SRMS, ΔN-SRMS or SRMS-K258M in HEK293 cells (Fig. 1*A*). We used general phosphotyrosine antibodies to probe the levels of tyrosine-phosphorylated proteins in the whole cell lysates derived from these cells. Our results confirmed that the ectopic expression of wild type SRMS but not ΔN-SRMS or SRMS-K258M lead to the tyrosine-phosphorylation of several endogenous proteins in these cells (Fig. 1*B*). The lysates were also probed with antibodies against GFP to ensure that the SRMS variants were expressed at similar levels in these cells (Fig. 1*B*). The tyrosine-phosphorylated proteins observed in wild type SRMS-expressing cells represent the potential substrates of SRMS. We previously reported DOK1 as one of the proteins that is tyrosine phosphorylated in SRMS-overexpressing HEK293 cells (6). However, the identity of the other tyrosine-phosphorylated proteins in these cells and the specific tyrosine residues potentially targeted by SRMS remains unknown.

Phosphoproteomics Workflow to Enrich Tyrosine-phosphorylated Targets by Immuno-affinity Purification—In order to identify the cellular substrates of SRMS, we performed a label-free quantitative phosphoproteomics approach to profile tyrosine-phosphorylated proteins in HEK293 cells ectopically expressing enzymatically active wild type SRMS (Fig. 2). We transiently transfected either GFP-tagged wild type SRMS or the empty vector as a control, in HEK293 cells in a large-scale experiment. We used the empty vector-expressing cells as a control to represent all steady state tyrosine phosphorylation events occurring natively in cells. A total of twelve 10 cm dishes were transfected with either GFP-wild type SRMS or the control vector backbone. Transfection efficiencies were determined to be over 90%. We harvested the cells directly in a strong denaturing lysis buffer and performed in-solution trypsin digestion of total proteins (Fig. 2). The crude tryptic peptides were desalted via reversed-phase solid-phase extraction and anti-phosphotyrosine antibodies were used to enrich for tyrosine phosphorylated peptides from cells expressing either GFP-SRMS or the empty vector control (Fig. 2). The enriched tyrosine-phosphorylated peptides, from both populations of cells, were then sequenced via LC-MS/MS (Fig. 2).

Identification of Candidate SRMS Substrates—Using the MaxQuant-Andromeda integrated platform and the Perseus quantitative analyses framework we applied quality thresholds (33, 35, 47, 48) to allow the identification of high-confidence phosphopeptides (Fig. 3). The search parameters on MaxQuant-Andromeda were adjusted using 1% FDR and quality Andromeda search and Delta scores were used as minimum thresholds (Fig. 3*A* and 3*B*, supplemental Tables S1 and S2). Using Pearson's correlation analysis, we observed good reproducibility of the phosphopeptides quantified from both biological replicates of each sample ($R \geq 0.8$, supplemental Fig. S1). We finally based subsequent analyses exclusively on class I phospho-sites that matched a reasonably stringent *t* test-based statistical threshold (*p* value < 0.05, Student's *t* test) (Fig. 3*C* and 3*D*, supplemental Table S3).

Using these criteria, our analyses led to the identification of a total of 1450 tyrosine- phosphorylated peptides pooled from both, SRMS-expressing and control cells (Fig. 4*A* and

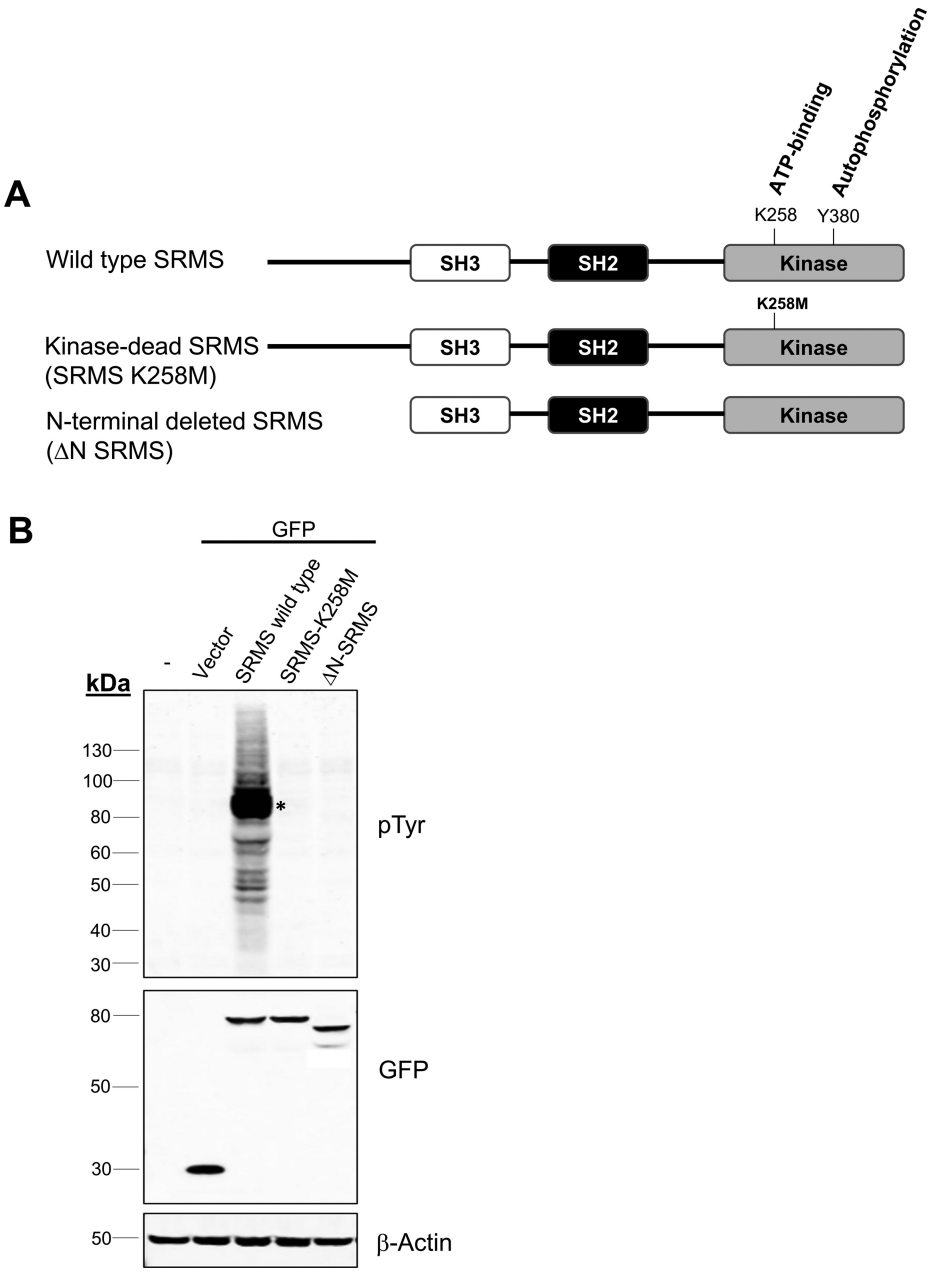

FIG. 1. **SRMS induces the tyrosine phosphorylation of several cellular proteins.** *A*, Shown here are the schematic domain-structure representations of the wild type SRMS protein, the kinase-dead SRMS mutant (K258M) and the N-terminal-deleted SRMS mutant (ΔN-SRMS) which lacks the first 50 amino acids in the N-terminal region of SRMS. Y380 represents the highly conserved autophosphorylation site within the activation loop of the SRMS kinase domain and K258 represents the conserved ATP-contacting residue in the ATP-binding pocket of the SRMS kinase domain. *B*, GFP-tagged SRMS constructs, namely, wild type SRMS, kinase-dead SRMS (SRMS- K258M) and ΔN-SRMS were transiently overexpressed in HEK293 cells. Untransfected HEK293 cells or HEK293 cells transfected with the empty vector encoding GFP alone, were used as controls. Post-transfection, the cells were lysed and the lysates probed with antibodies against total tyrosine phosphorylated residues (pTyr), GFP and β-actin. Immunoblotting with β-actin was used as a control for protein loading. Asterisk represents the approximate position of auto-phosphorylated GFP-wild type SRMS.

supplemental Table S3). Of these, 1258 peptides were unique and mapped to 771 distinct proteins (Fig. 4*A* and supplemental Table S3). A total of 141 peptides were found to be conserved in more than one protein and such proteins were consequently clustered in the respective protein groups by MaxQuant (supplemental Table S3). As expected, we identified a far greater number of tyrosine-phosphorylated peptides in SRMS-overexpressing cells compared with control cells (Fig. 4*B*, left panel). This observation was consistent with our findings from Fig. 1*B* as well as additional immunoblotting analyses where we used general phosphotyrosine antibodies to assess total tyrosine-phosphorylated proteins in the same pool of lysates which were used toward mass spectrometry analyses (Fig. 4*B*, right panel). Although SRMS-overexpressing cells readily exhibited a significant number of tyrosine-phosphorylated proteins, longer exposures of the immunoblot revealed a fair but comparatively lower number of tyrosine-phosphorylated proteins in the control cells as well (supplemental Fig. S2). This is expected because tyrosine phosphorylation occurs natively in cells although at a far lower biological stoichiometry compared with serine/threonine phosphorylation events (49, 50).

Of the 1258 unique tyrosine-phosphorylated peptides identified between both samples, 1129 phosphopeptides were identified exclusively in SRMS-expressing cells whereas only 117 phosphopeptides were enriched in the control cells

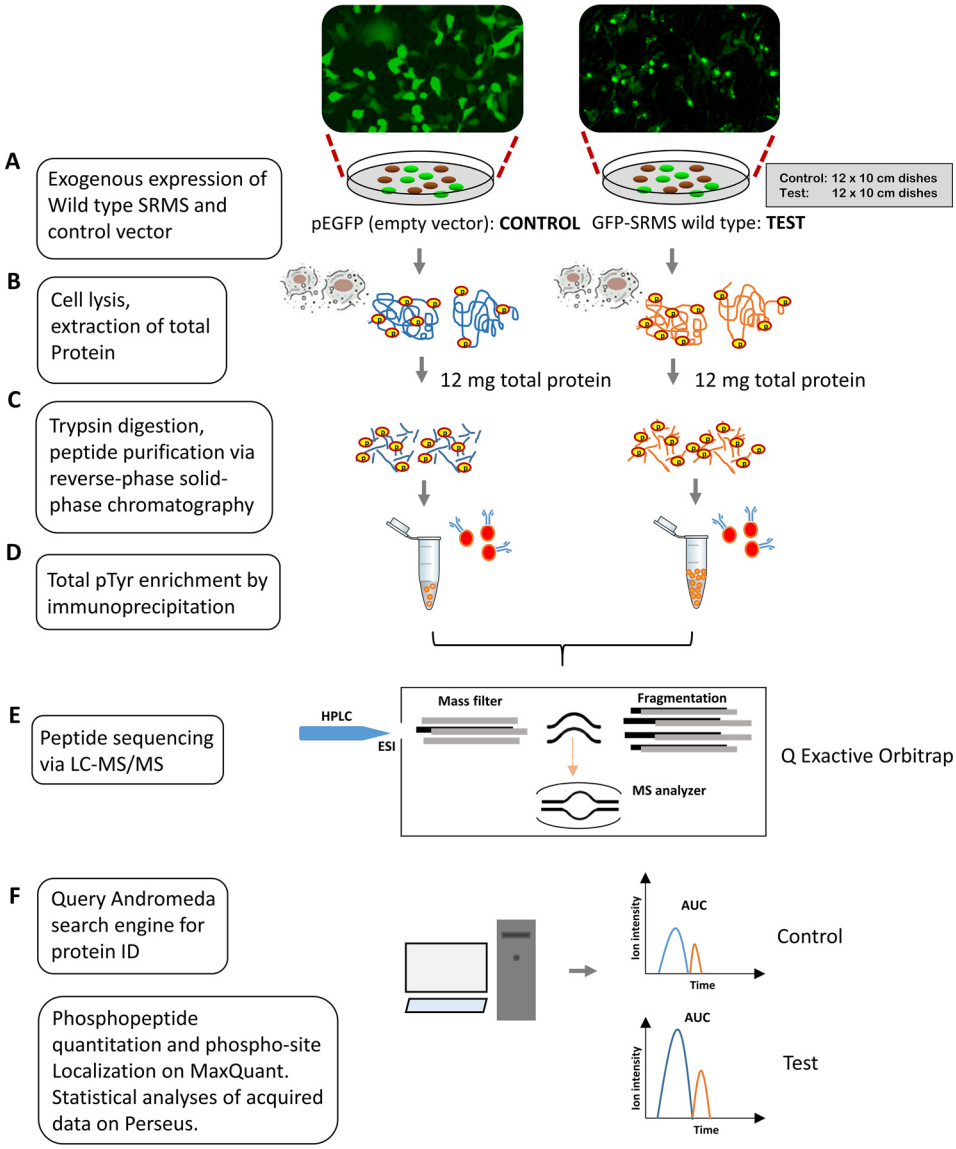

FIG. 2. **Experimental workflow.** A label-free quantitation-based mass spectrometry approach was adopted to identify the candidate cellular substrates of SRMS. *A*, Plasmid constructs encoding either GFP-tagged wild type SRMS or GFP alone (empty vector) were exogenously introduced in HEK293 cells. *B*, 24 h post-transfection the cells were lysed under denaturing conditions. *C*, 12 mg total protein, each from GFP alone and GFP-SRMS conditions, was trypsin-digested and the crude tryptic peptides were desalted via reversed-phase solid-phase chromatography. *D*, The desalted peptides were then used toward immunoprecipitation of total tyrosine-phosphorylated peptides. *E*, The enriched tyrosine-phosphorylated peptides from each condition were sequenced via LC-MS/MS. All fractions were separated using a 2-hour a reversed-phase gradient and electro-sprayed into a Q Exactive HF quadrupole instrument. *F*, Protein IDs and phospho-site localization were determined using the MaxQuant platform which integrates the Andromeda search engine. The entire workflow was performed in 2 biological replicates.

(Fig. 4*B*, left panel and supplemental Table S3). Additionally, 99 phosphopeptides were found common to both SRMS-expressing and control cells (Fig. 4*B*, right panel and supplemental Table S3). We considered the tyrosine-phosphorylated targets as candidate substrates of SRMS only if the corresponding phosphopeptides were exclusively enriched in the SRMS overexpressing cells at a p value threshold of 0.05 between the replicates. All tyrosine-phosphorylated peptides identified in the control cells were considered background phosphorylation events. Because none of the phosphopeptides identified as common to SRMS-overexpressing and control cells displayed at least 2-fold differential abundance in phosphopeptide intensities, we reasoned that proteins mapped from these peptides would be less likely to represent candidate SRMS substrates and were therefore filtered. Using this approach, we identified 663 candidate SRMS substrates across two biological replicates with a p value <0.05 (Fig. 4*B*, left panel and supplemental Table S3). A subset of the SRMS

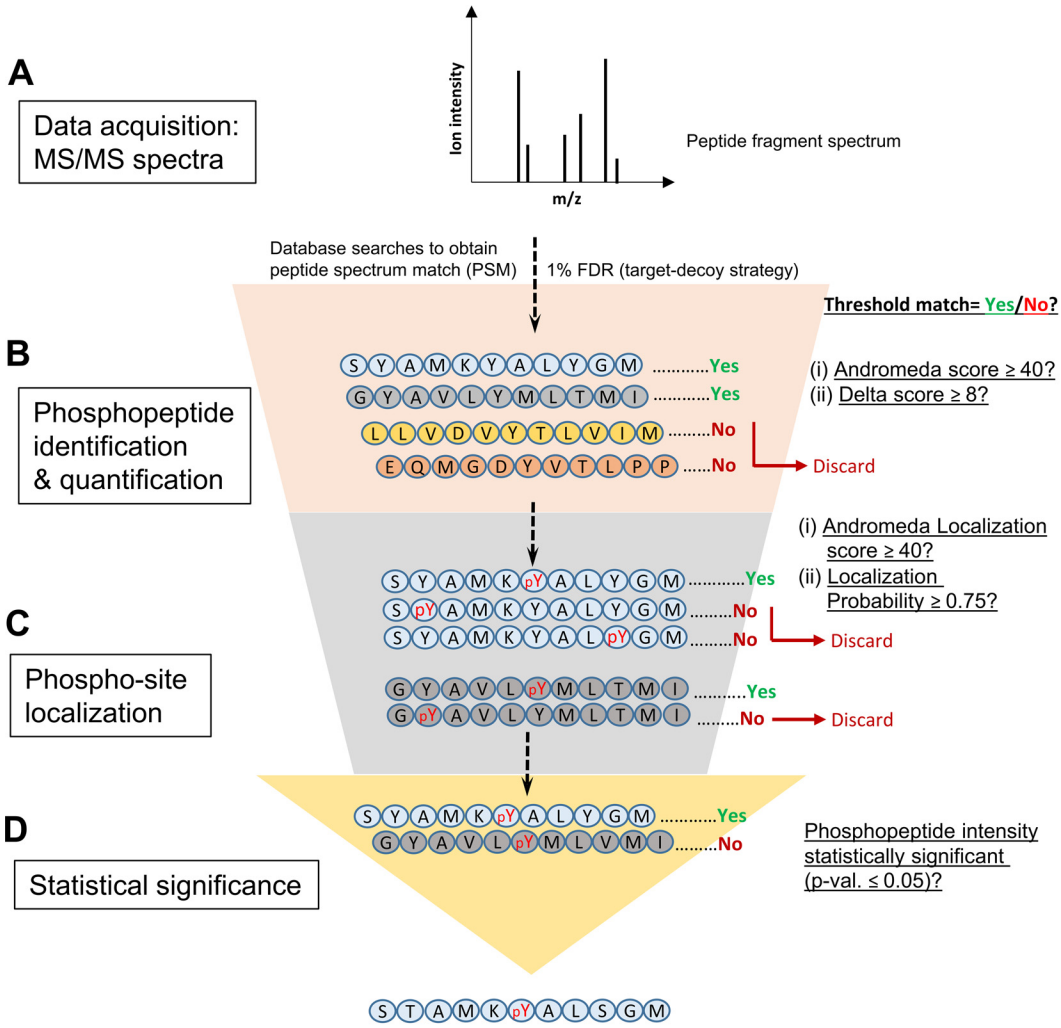

FIG. 3. **Flowchart depicting the computational pipeline used to identify high confidence phosphopeptides.** *A*, The acquired raw instrument data were processed on the MaxQuant-Andromeda platform that integrates the Perseus software for data quantitation. Each peptide spectrum obtained was queried using the Andromeda search engine to generate reliable peptide-spectrum matches (PSM) against the queried database. Peptide sequences and protein IDs were assigned at 1% False Discovery Rate (FDR), based on target-decoy searches. *B*, Phosphopeptides were quantified based on their pre-cursor ion intensities, calculated as the area of the associated peak or area-under-the curve (AUC). Phosphopeptides with an associated "Andromeda score" < 40.0 and Delta score < 8 were discarded. *C*, Class I phospho-sites were selected with an "Andromeda "localization score" and "localization probability" threshold of 40.0 and 0.75, respectively. *D*, Finally, a statistical *t* test threshold was applied to the identified phosphopeptides. Only phosphopeptides with corresponding pre-cursor ion intensities that were statistically significant, with a p value ≤ 0.05 between both biological replicates, were retained. "Threshold match = Yes" indicates that the phosphopeptide(s) matched the threshold for the above parameters and were accepted. "Threshold match = No" indicates that the phosphopeptides failed to match the threshold for the parameters and were discarded.

candidate substrates is listed in Table I. Importantly, our phosphoproteomics analyses identified DOK1 as a hyper-phosphorylated target in wild type SRMS-expressing cells. This was an important observation because we previously validated DOK1 as a direct substrate of SRMS and showed that the exogenous expression of SRMS led to the phosphorylation of endogenous DOK1 in HEK293 cells (6). Our MS analyses therefore validated our previous findings. The SRMS Y380 residue represents a key autophosphorylation site within the kinase domain activation loop and is essential for SRMS enzymatic activity (6). As expected, the peptide corresponding to SRMS Y380 was identified as one of the major phosphopeptides from our MS analyses. Additionally, we identified 14 other tyrosine- phosphorylated sites in SRMS that were not previously known (Table I).

We also assessed the multiplicity of phosphorylation associated with tyrosine residues in the identified tyrosine-phosphorylated peptides. We found that most of the tyrosine-phosphorylated peptides, identified between both samples, were singly phosphorylated (Fig. 4*C*). However, the singly

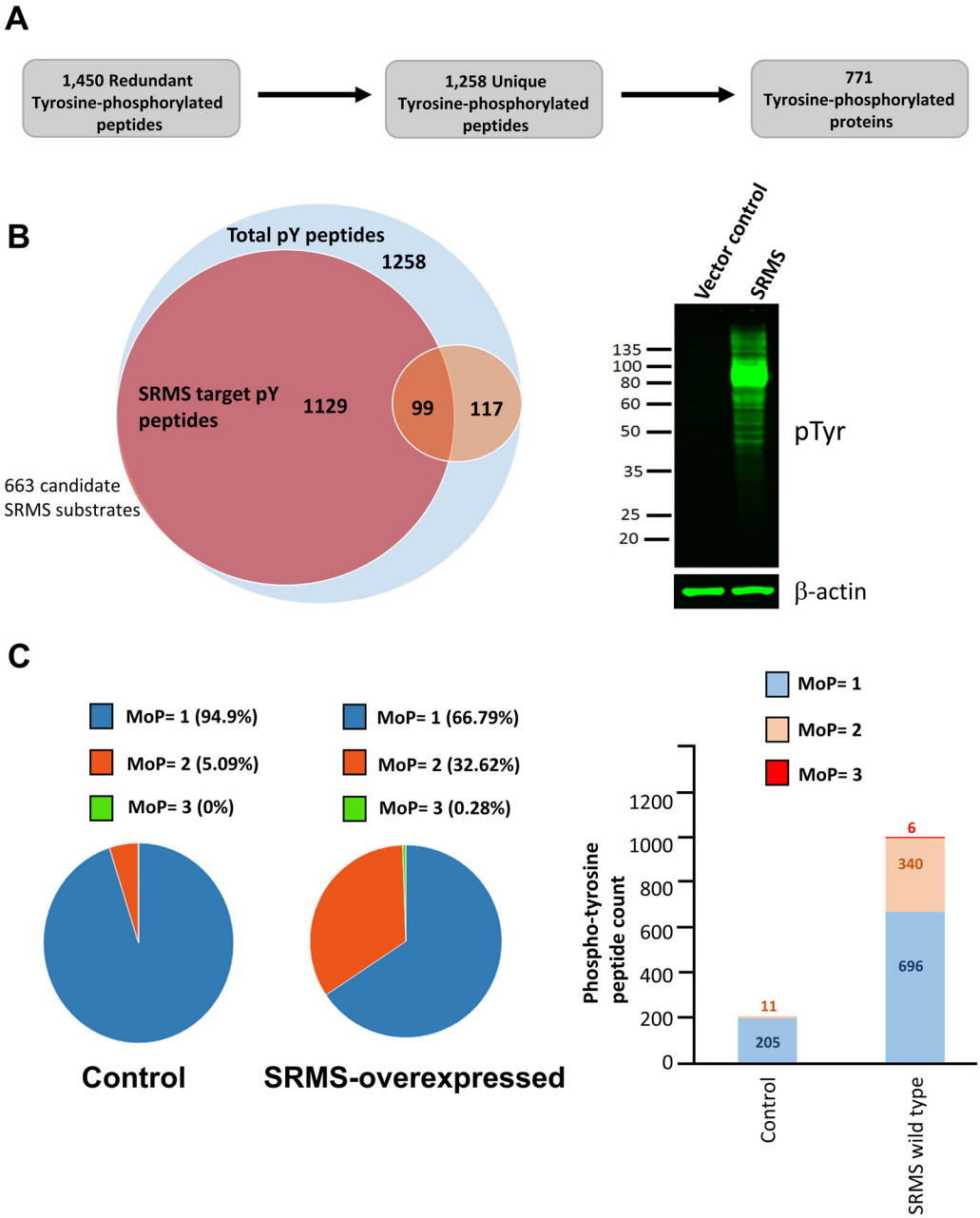

FIG. 4. **Overview of the identified tyrosine-phosphoproteome.** *A*, The MaxQuant-Andromeda platform quantified a total of 1450 redundant tyrosine-phosphorylated peptides from both control and SRMS-overexpressing cells. Of these, 1258 tyrosine-phosphorylated peptides were unique and mapped to 771 unique proteins. *B*, A Venn diagram depicts the number of tyrosine-phosphorylated peptides either unique to SRMS-overexpressing cells, control cells or common to both. Of the 1258 unique tyrosine-phosphorylated peptides identified globally, 1129 peptides were enriched exclusively in SRMS-overexpressing cells whereas 117 peptides were identified exclusively in control cells. 99 peptides were found common to both samples (left panel). The 1129 phosphopeptides identified exclusively in SRMS-expressing cells mapped to 663 proteins. Prior to trypsinization, 25 μg whole cell lysates derived from large-scale transfections of HEK293 cells, were probed with general phosphotyrosine antibodies via immunoblotting analyses to confirm the expression of tyrosine-phosphorylated proteins resulting from SRMS kinase activity (right panel). *C*, The tyrosine-phosphorylated peptides were segregated based on multiplicity of phosphorylation (MoP). Singly- (MoP = 1), doubly- (MoP = 2) or triply- (MoP = 3-phosphorylated peptides were quantified and represented either as percent-abundance of total tyrosine-phosphorylated peptides in each sample (pie-chart, left panel) or in absolute numbers (right panel).

phosphorylated peptides were significantly more abundant (>3-fold) in SRMS-expressing cells compared with control cells (Fig. 4*C*). Interestingly, doubly-phosphorylated peptides were over 30-fold more abundant in SRMS-expressing cells compared with control cells (Fig. 4*C*). Additionally, though detected only as a minor proportion, triply-phosphorylated peptides were identified in SRMS-expressing cells but not in the control cells (Fig. 4*C*). The greater multiplicity of phos-

TABLE I
List of selected candidate SRMS substrates and associated phospho-sites identified via quantitative phosphoproteomics

Protein Name	Uniprot ID	Phospho-site(s) identified
SRMS (Src-related kinase lacking C-terminal regulatory tyrosine and N-terminal myristoylation sites)	Q9H3Y6	Y87, Y121, Y156, Y169, Y180, Y196, Y197, Y299, Y340, Y380, Y400, Y422, Y427, Y456, Y443
Vimentin	PO8670	Y61, Y383
EIF2S1 (Eukaryotic translation initiation factor 2 subunit 1)	G3V4T5	Y109
MAGED1 (Melanoma-associated antigen D1)	Q9Y5V3	Y92, Y136, Y161, Y423, Y426, Y429, Y487, Y609, Y505, Y509
VDAC2 (Voltage-dependent anion-selective channel protein 2)	P45880	YY73, Y78, Y236, Y258
ABLIM1 (Actin-binding LIM protein 1)	F8W8M4	Y313
Dok1 (Docking protein 1)	Q99704	Y337, Y341, Y398, Y409
Sam68	Q07666	Y167
MICOS(MICOS complex subunit MIC60)	B9A067	Y33, Y589
MCM7 (DNA replication licensing factor MCM7)	P33993	Y6, Y33
MCM4 (DNA replication licensing factor MCM4)	P33991	Y421
DNAJB6 (DnaJ homolog subfamily B member 6)	C9JDR7	Y68
DDX5 (Probable ATP-dependent RNA helicase DDX5)	J3KTA4	Y442, Y514, Y518
DNAJC7 (DnaJ homolog subfamily C member 7)	Q99615	Y38, Y65, Y221, Y222, Y272, Y276, Y279, Y297, Y355
PKP2 (Plakophilin-2)	Q99959	Y88

phorylation observed on individual peptides in SRMS-expressing cells, indicates that SRMS likely phosphorylates its substrates on several tyrosine residues.

In Silico Analyses Identifies Candidate SRMS Substrate Motifs—As described above, our analyses revealed 1129 non-redundant tyrosine-phosphorylated peptides in SRMS-overexpressing cells. We were interested in identifying candidate SRMS substrate motifs to understand the pattern of substrate-specificity exhibited by the SRMS kinase domain. Motif-specificities exhibited by tyrosine kinase domains are less understood compared with the other well-characterized modular domains such as the SH3, SH2 and PTB domains, primarily because the cellular substrates of several of these kinases are unknown. To identify the consensus sequence(s) of SRMS substrates, we used the entire pool of unique phosphopeptides ($n = 1129$) derived from the 663 candidate SRMS substrates, enriched exclusively from SRMS-overexpressing cells. We performed motif-analyses using two well described and popular *in silico* tools, namely, Motif-x (52) and MMFPh (Maximal motif finder for phosphopeptides) (51). The active site of kinases is known to recognize residues that are immediately N-terminal and/or C-terminal to the phosphoacceptor site, implying that consensus sequences are generally short (19). We therefore refined the length of our query phosphopeptides to 13 amino acids. Using Motif-x, we identified six major classes of putative SRMS substrate consensus motifs at a significance threshold of 10^{-6} (Fig. 5*A* and supplemental Table S4). Interestingly, the top three consensus sequences identified by Motif-x were also reported as over-represented by the other *in silico* tool, MMFPh (Fig. 5*B*). Additionally, analyses using MMFPh revealed three other candidate consensus sequences that were not reported by Motif-x (supplemental Fig. S3 and supplemental Table S4).

Overall, motif-analyses using these two programs revealed that top SRMS candidate consensus sequences predominantly displayed a lysine residue at either the −2 (*KxY,* where Y represents the phosphorylated tyrosine residue at position "0" and "x" is any amino acid residue) or −4 position (*KxxxY*)

A

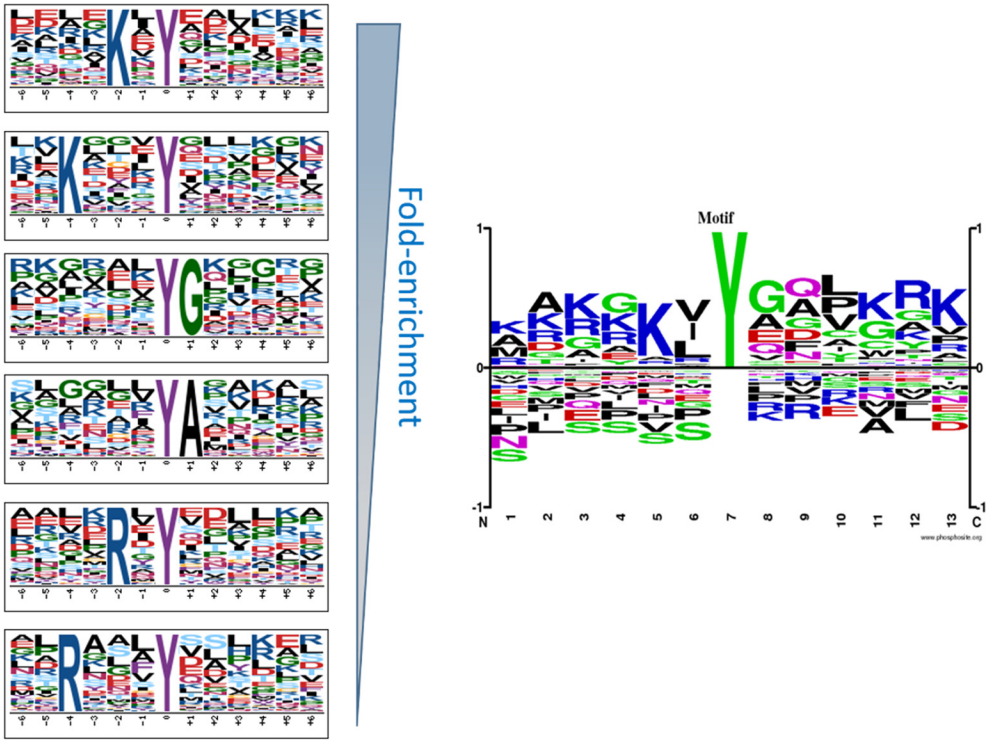

B

Motif	Foreground matches	Background size	Fold increase	Score
KxY	219	322611	3.1	16.0
KxxxY	107	301665	2.28	14.32
YG	104	285335	2.15	12.50

Motif-x

Motif	Foreground matches	Background size	Ratio	Score
KxY	227	46530	4.9E-3	1.602
KxxxY	121	37228	3.3E-3	1.016
YG	134	42575	3.1E-3	0.969

MMFPh

FIG. 5. **Analyses of candidate SRMS consensus motifs.** *A*, The *in silico* motif analyses tool motif-X (52) was used to assess overrepresented motif patterns in tyrosine-phosphorylated peptides ($n = 1129$) derived from 663 candidate SRMS substrates. Six candidate consensus motifs, identified as significantly enriched, are represented in individual motif logos (left panel). A representative motif logo of all candidate SRMS consensus motifs was generated using the Phosphosite motif analyses tool (http://www.phosphosite.org/sequenceLogoAction) (right panel). The size of the amino acid letter, in the motif logo (left and right panels), is proportional to the magnitude of overrepresentation of this residue in the pool of queried peptides. *B*, The tables represent statistical information on the SRMS candidate consensus motifs identified using either the motif-x (52) or MMFPh (51) tools. Foreground matches indicate the number of queried peptides that correspond to the identified motif. Background size indicates the background pool of phosphopeptides used as reference. The algorithmically determined scores associated with each motif are indicated.

(Fig. 5*A* and 5*B*). Another overrepresented candidate consensus motif displayed a glycine at the +1 position (*YG*) (Fig. 5*A* and 5*B*). Other enriched motifs contained either a lysine residue at +6 (*YxxxxxK*), valine at −1 (*VY*) or a glutamic acid at +1 (*YE*) positions, respectively (supplemental Fig. S3). We also examined the possibility that the more rigorous SRMS substrate consensus motifs would likely be represented by a subset of phosphopeptides enriched at significantly higher relative abundances. To address this, we performed motif-analyses using 86 phosphopeptides, corresponding to candidate SRMS substrates, that were quantified with average log2 ion intensities of at least 24.0. Using the Motif-x tool, we consistently identified the *KxY* motif as the most overrepresented consensus sequence among the queried phosphopeptides, implying that this may likely represent one of the major SRMS kinase consensus motifs (supplemental Fig. S4).

Functional Gene Enrichment Analysis of Candidate SRMS Substrates—The cellular and physiological role of SRMS is poorly understood. To gain insights into the biological function of SRMS, we performed pathway enrichment analyses on the candidate SRMS substrates using the g:Profiler software (41). To complete a high-confidence pathway analysis and restrict our enrichment analysis solely to phosphoproteins, we used a custom background set of all reported phosphoproteins curated with the PhosphositePlus database (42). This increased the stringency at the level of the expected number of proteins associated with every Gene Ontology (GO)-annotated pathway identified. We further filtered low-confidence GO annotations of genes that had been only derived from automated computational analysis. Our analysis revealed 176 significantly enriched biological pathways and processes (FDR$<$0.05) that associated with a large fraction (411/663 proteins or 62%) of the candidate SRMS substrates (Fig. 6*A* and 6*B* and supplemental Table S5). We constructed an enrichment map visualization (43) and manually annotated subnetworks of similar pathways as functional themes (Fig. 6*B*). We found that the top pathways and processes associated with the candidate SRMS substrates included themes such as proteolysis and protein ubiquitination (*e.g.* negative regulation of protein ubiquitination, FDR = 5×10^{-11}, 31 proteins), mitotic cell cycle (*e.g.* cell cycle phase transition, FDR = 3×10^{-11}, 66 proteins), cellular energy metabolism (*e.g.* ATP metabolic process, FDR = 4×10^{-8}, 36 proteins) and RNA processing (*e.g.* RNA catabolic process, FDR = 8×10^{-12}, 54 proteins) (Fig. 6*A* and 6*B*). Several other interesting themes with fewer pathways were also apparent, such as regulation of stem cell differentiation (FDR = 0.03, 16 proteins) and cellular response to hypoxia (FDR = 0.004, 21 proteins). Two themes corresponding to established signal transduction pathways were also significantly enriched: Wnt signaling pathway (FDR = 9×10^{-4}, 18 proteins) and tumor necrosis factor (TNF)-mediated signaling pathway (FDR = 4×10^{-3}, 20 proteins). Overall, pathway enrichment analyses of our phosphoproteomics dataset revealed several distinct and related cellular processes potentially regulated by SRMS in a kinase-dependent manner.

Validation of Candidate SRMS Substrates Using Peptide Arrays—Our mass spectrometry-based phosphoproteomics analyses identified 663 candidate SRMS substrates (Fig. 4*A* and 4*B*). We decided to utilize peptide microarrays in a complementary approach to perform high-throughput validation of a subset of the candidate SRMS substrates. Peptide microarrays are robust and versatile tools that have been previously used for screening kinase-substrates (54), identifying kinase substrate-motifs (55) and investigating phosphoproteome-based signaling in eukaryotic cells (56). We generated a customized peptide array comprising 102 unique peptides (supplemental Table S6). Of these, 100 peptides were derived from the tyrosine-phosphorylated peptides identified in our MS analyses (supplemental Table S6). These 100 peptides included 80 test peptides corresponding to 58 candidate SRMS substrates that were identified exclusively in SRMS-expressing cells at log2 intensities $>$20 and 20 negative control peptides that were selected randomly (supplemental Table S6). Of these 20 negative control peptides, 9 were identified in our MS analyses from control cells alone and 11 were common to both SRMS-expressing and control cells (supplemental Table S6). The remaining two are control peptide, a negative control peptide corresponding to Beclin1 Y352 that was previously reported as a direct phosphorylation site for EGFR but not SRMS (57), and a peptide corresponding to the BRK Y447 residue because this was recently reported as a site that is directly phosphorylated by SRMS (11). Each peptide was printed in three triplicate sets (9 peptide replicates in total) on each array to allow for intra-array normalization (40, 58) of the peptide phosphorylation intensities.

We used lysates derived from HEK293 cells overexpressing either GFP-SRMS wild type or GFP-kinase-dead SRMS to assess the phosphorylation status of the peptides on the microarrays. Data from our peptide microarray analyses showed that compared with arrays treated with kinase-dead SRMS, wild type SRMS-treated arrays displayed increased phosphorylation of 52 peptides derived from candidate 44 candidate SRMS substrates (fold change phosphorylation $>$ 1) (supplemental Table S7). Of these, 26 peptides, derived from 24 candidate substrates showed a SRMS kinase-dependent increase in tyrosine phosphorylation across all technical replicates (p value = 0.003–0.09) (supplemental Table S8). A subset of these validated targets is represented in Table II and Fig. 7. As expected, none of the 21 control peptides, including Beclin1 Y352, showed increased phosphorylation in the wild type SRMS-treated arrays compared with kinase-dead SRMS-treated arrays (supplemental Table S7 and S8). Importantly, we observed an increase in the phosphorylation of the peptide corresponding to DOK1 Y337, in wild type SRMS-treated arrays compared with kinase-dead SRMS-treated arrays (Table II and supplemental Table S7 and S8). This again corroborates our previous findings where we

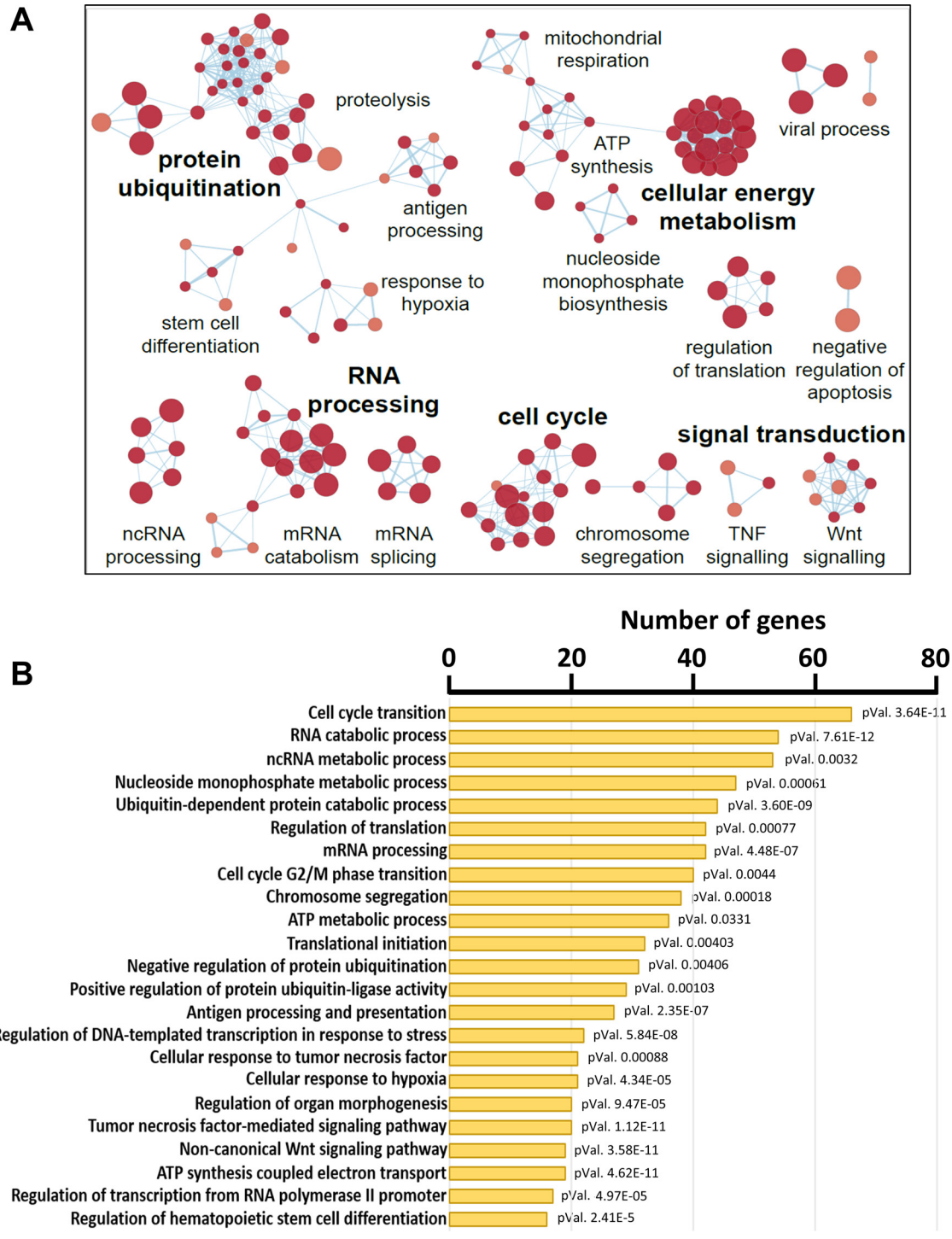

FIG. 6. **Functional gene enrichment analyses of candidate SRMS substrates.** *A*, Enrichment map of significantly enriched cellular processes and pathways enriched by candidate SRMS substrates (FDR<0.05). Network nodes represent enriched pathways and edges connect pathways with many shared genes. Biological themes associated with groups of nodes represent a simplified summary of multiple related pathways and were assigned through manual curation. The size of each node is proportional to the number of genes involved in the given pathway or process. *B*, Barplot shows the most significant pathways and processes and number of associated proteins enriched among SRMS substrates. The adjusted *p* value associated with each annotated process/pathway is indicated.

TABLE II
Top SRMS targets validated on peptide arrays

S. no.	Peptide corresponding to protein	UniProtKB ID	p-Tyr. site	Fold-change phosphorylation	pValue	Candidate SRMS substrate Motif
1	Vimentin (VIM)	P08670	Y383	1.94436	0.021	*xx**RxY**xx*
2	Guanine nucleotide-binding protein subunit beta-2-like 1, N-terminally processed (GNB2L1)	P63244	Y246	1.84406	0.013	--
3	Cytoskeleton-associated protein 2 (CKAP2)	Q8WWK9	Y592	1.73666	0.005	--
4	Cyclin-dependent kinase 2/3 (CDK2/3)	G3V5T9	Y19	1.68668	0.031	*xx**VY**xx*
5	Heterogeneous nuclear ribonucleoprotein M (HNRNPM)	P52272	Y681	1.53786	0.008	*xx**YA**xx*
6	Eukaryotic initiation factor 4A-III/ 4A-I (EIF4A3/1)	P38919	Y50	1.53058	0.038	xx**YG**xx
7	Uridine 5-monophosphate synthase (UMPS)	P11172	Y326	1.48503	0.071	*xx**KxY**xx*
8	Keratin, type I cytoskeletal 18 (KRT18)	F8VZY9	Y94	1.45291	0.089	--
9	UBX domain-containing protein 6 (UBXN6)	Q9BZV1	Y181	1.43765	0.050	--
10	Guanine nucleotide-binding protein-like 3-like protein (GNL3L)	Q9NVN8	Y243	1.41008	0.059	--
11	Melanoma-associated antigen D1 (MAGED1)	Q9Y5V3	Y505	1.37761	0.002	*xx**RxY**xx*
12	40S ribosomal protein S3 (RPS3)	P23396	Y87	1.36634	0.015	*xx**YA**xx*
13	Docking protein 1 (Dok1)	Q99704	Y337	1.33743	0.059	*xx**KxxY**xx*
14	DNA replication licensing factor MCM7	P33993	Y33	1.32199	0.032	*xx**YG**xx*
15	Growth factor receptor-bound protein 10 (GRB10)	Q13322	Y354	1.31135	0.090	*xx**KxY**xx*
16	Guanine nucleotide exchange factor VAV2	P52735	Y552	1.28324	0.068	--

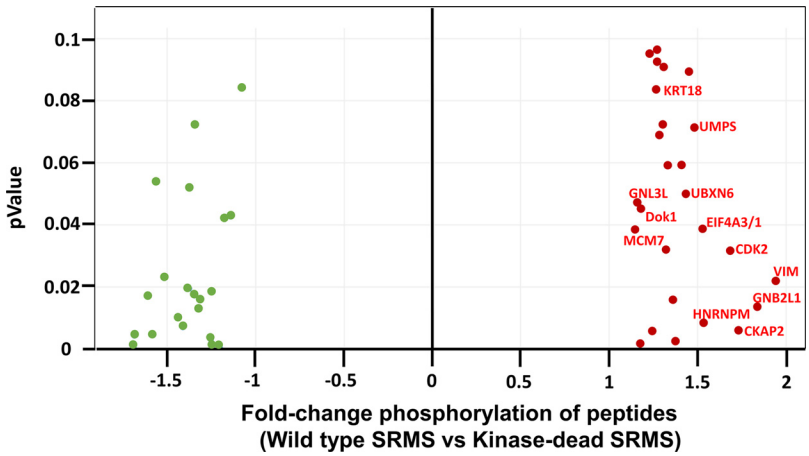

FIG. 7. **Validation of target peptides using peptide microarrays.** A scatter plot of differentially phosphorylated peptides between wild type SRMS-treated and kinase-dead SRMS-treated conditions. Peptides highlighted in red represent hyperphosphorylated targets identified in arrays treated with wild type SRMS. (*p* value range 0.003–0.09). Selected hyperphosphorylated peptides are labeled in the scatter plot.

identified DOK1 as a *bona fide* SRMS substrate (6). We also observed a modest increase in the phosphorylation of the BRK Y447 peptide in arrays treated with lysates of cells overexpressing wild type SRMS. The BRK Y447 peptide showed 1.2-fold increased phosphorylation in wild type SRMS-treated arrays compared with kinase-dead SRMS-treated arrays (supplemental Tables S7 and S8). Additionally, we found that the top target peptides validated in our phosphorylation assays displayed motifs that matched the candidate consensus motifs for SRMS (Table II), as determined through *in silico* analyses (Fig. 5 and supplemental Fig. S2). These included motifs, *RxY* (VIM Y383 and MAGED1 Y505),

VY (CDK2/3 Y19), *KxY* (UMPS Y326 and GRB10 Y354), *KxxY* (DOK1 Y337), *YA* (HNRNPM Y681 and RPS3 Y87) and *YG* (EIF4A3 Y50 and MCM7 Y33).

Validation of Vimentin and Sam68 as SRMS Substrates—Our peptide array analyses revealed vimentin as a top candidate substrate of SRMS (Table II and Fig. 7). Vimentin (VIM) is a key cytoskeletal protein and a substrate of c-Src and various serine/threonine kinases (59–61). Interestingly, KHDRBS1/Sam68 was also identified as a candidate SRMS substrate from our MS analyses although this was not tested in our peptide microarrays. Sam68 is a key RNA-binding protein implicated in cellular RNA-metabolic processes whose functions are regulated by phosphorylation (62). We have previously shown that the SRMS family member, BRK phosphorylates Sam68 and regulates its RNA-binding properties (30). To verify vimentin and Sam68 as *in vivo* SRMS substrates, we performed immunoprecipitation analyses using GFP-vimentin and Myc-Sam68 constructs. We first coexpressed GFP-vimentin with either Flag-tagged wild type SRMS or SRMS K258M in HEK293 cells. Vimentin was immunoprecipitated using antibodies against GFP and the immunoprecipitates and input probed with antibodies against GFP, Flag or total phospho-tyrosines (Fig. 8*A* and 8*B*). Firstly, our immunoblotting analyses using antibodies against Flag-tag showed that both, wild type SRMS and SRMS K258M coprecipitated with ectopically expressed vimentin indicating that SRMS associates with vimentin in a kinase-independent manner (Fig. 8*A*). We observed the tyrosine-phosphorylation of vimentin only in wild type SRMS-transfected cells and not SRMS K258M-transfected cells, confirming that the phosphorylation of vimentin is SRMS kinase-dependent (Fig. 8*A*). Likewise, we coexpressed Myc-Sam68 with either GFP-tagged wild type SRMS or SRMS-K258M. We immunoprecipitated Sam68 using antibodies against Myc and probed the immunoprecipitates and input using antibodies against Myc, GFP and total phosphotyrosines (Fig. 8*C* and 8*D*). As seen with vimentin, we found that both, wild type SRMS as well as SRMS K258M coprecipitated with Sam68, indicative of kinase-independent pattern of intermolecular association (Fig. 8*C*). Importantly, Sam68 was found to be tyrosine phosphorylated only upon coexpression with wild type SRMS but not kinase-dead SRMS (Fig. 8*C*). Together, our findings concur with the results of our peptide array analyses and show that both vimentin and Sam68 are substrates of SRMS.

To test if vimentin and Sam68 are direct substrates of SRMS, we performed *in vitro* kinase assays using purified recombinant GST-SRMS kinase protein and GST-vimentin or GST-Sam68 proteins. Our results showed that in the presence of ATP, SRMS kinase directly phosphorylated both vimentin and Sam68 *in vitro* (Fig. 8*E* and 8*F*). As expected, in the absence of SRMS, vimentin and Sam68 were not phosphorylated. As an additional control, we incubated the GST protein alone with GST-SRMS kinase and observed no phosphorylation of the GST protein confirming that SRMS directly phosphorylates both, vimentin and Sam68 (Fig. 8*E* and 8*F*).

Because we found that vimentin and Sam68 coprecipitated with SRMS in our immunoprecipitation analyses, we asked if SRMS colocalizes with vimentin or Sam68 *in vivo*. To examine this, we cotransfected GFP-vimentin or GFP-Sam68 with either mCherry-wild type SRMS or SRMS K268M, in HEK293 cells and assessed colocalization by confocal microscopy analyses. Firstly, we observed that GFP-tagged or untagged wild type SRMS localized predominantly to cytoplasmic punctae (Fig. 9*A* and 9*B*), as we previously reported (6). Vimentin was predominantly found to localize to cytoplasmic tubular networks (Fig. 9*D*), consistent with previous reports describing these as vimentin intermediate filaments (VIFs) (63, 64). Importantly, we observed that GFP-vimentin and mCherry-wild type SRMS colocalized in the cytoplasm of HEK293 cells (Fig. 9*E*). We tested this colocalization reciprocally using GFP-wild type SRMS and mCherry-vimentin constructs. We observed that both mCherry-vimentin and GFP-SRMS colocalized in the cytoplasm (Fig. 9*F*). We also noted that SRMS colocalized with vimentin in VIFs rather than in the characteristic SRMS-cytoplasmic puncta, indicating that vimentin likely sequesters SRMS to VIFs (Fig. 9*E* and 9*F*). No colocalization was observed between mCherry alone and GFP-vimentin, implying that the observed colocalization between SRMS and vimentin does not depend on the fluorescent protein tags used (Fig. 9*G*).

Although Sam68 is known to localize predominantly to the nucleus (30, 65), certain studies have reported a cytoplasmic localization of the RNA-binding protein (66–68). Consistent with previous reports, we found that Sam68 localized predominantly to the nucleus when expressed alone or coexpressed with mCherry (Fig. 9*H* and 9*I*). However, in a few cells we also observed a partial cytoplasmic localization of Sam68 (Fig. 9*I*). This partial cytoplasmic localization was observed when GFP-Sam68 was expressed either alone or coexpressed with an empty vector encoding the mCherry protein. Coexpression of GFP-Sam68 and mCherry-SRMS revealed partial colocalization of both proteins where SRMS colocalized with cytoplasmic Sam68 (Fig. 9*J*). No colocalization was observed between GFP-Sam68 and mCherry alone (Fig. 9*I*). Together, our data show that both, vimentin and Sam68 colocalize with SRMS in the cytoplasm.

SRMS Induces the Tyrosine Phosphorylation of Sam68 in an EGF-dependent Manner—Sam68 is known to be frequently tyrosine phosphorylated, which is essential for the regulation of the RNA-binding function of the protein (69). Because we found that Sam68 is a SRMS substrate, we checked if SRMS was required for the tyrosine-phosphorylation of Sam68 at the endogenous level. We used MDA-MB 231 cells because this cell line is known to express both proteins endogenously (6). To determine whether endogenous SRMS promotes the phosphorylation of Sam68, we transiently knocked-down SRMS and immunoprecipitated endogenous Sam68 from

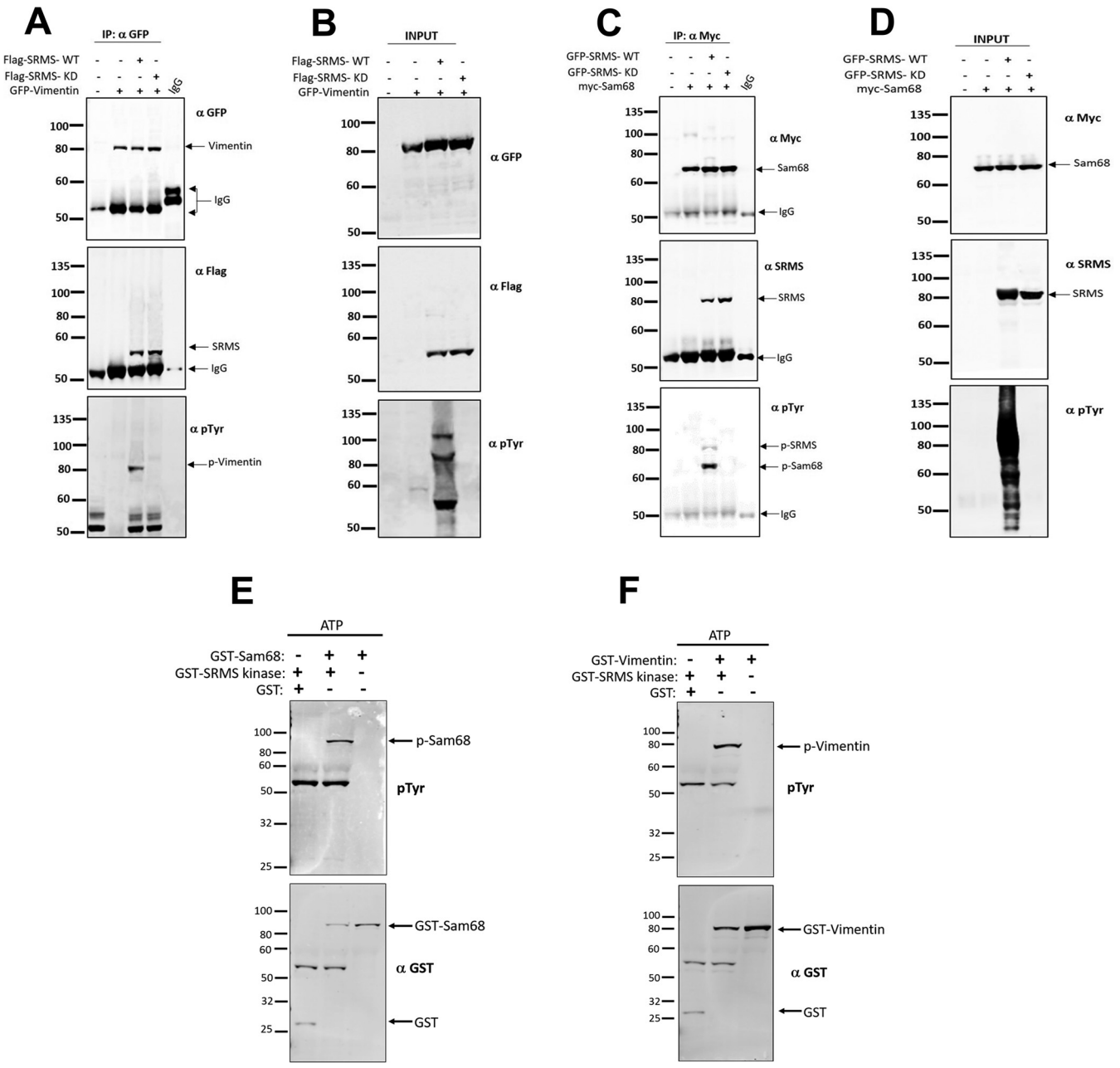

FIG. 8. **Validation of vimentin and Sam68 as SRMS substrates.** *A*, HEK293 cells were transiently transfected with constructs encoding GFP-vimentin alone or together with Flag-wild type SRMS (SRMS WT) or Flag-Kinase-dead SRMS (SRMS KD). GFP-vimentin was immunoprecipitated using antibodies against GFP. The immunoprecipitates (right panel) were probed with antibodies against GFP (top), Flag (Middle) or total phosphotyrosines (Bottom). *B*, Input from the corresponding lysates were probed with the same antibodies and are shown in the same order (Right panel). *C*, HeLa cells were transfected either individually with Myc-Sam68 or cotransfected with GFP-wild type SRMS or GFP-kinase-dead SRMS. Myc-Sam68 was immunoprecipitated using anti-myc antibodies. The immunoprecipitates (left panel) were probed with antibodies against Myc (top), GFP (middle) or total phosphotyrosines (bottom). *D*, Input from the corresponding lysates were probed with the same antibodies and are shown in the same order (Right panel). *E*, *In vitro* kinase assays were performed using purified recombinant GST-SRMS kinase and GST-Sam68. GST-Sam68 was incubated with or without GST-SRMS kinase and in the presence of ATP. GST-SRMS kinase was also incubated with GST alone as a control. Phosphorylation of Sam68 by SRMS was assessed by Western blotting using general phosphotyrosine antibodies. The immunoblots were also probed with antibodies against GST to show the expression of the GST-Sam68, GST-SRMS kinase and GST alone. *F*, Purified recombinant GST-vimentin was incubated with or without GST-SRMS kinase and in the presence of ATP. Phosphorylation of vimentin by SRMS was assessed by Western blotting using general phosphotyrosine antibodies. GST-SRMS kinase was also incubated with GST alone as a control. The immunoblots were also probed with antibodies against GST to show the expression of the respective proteins.

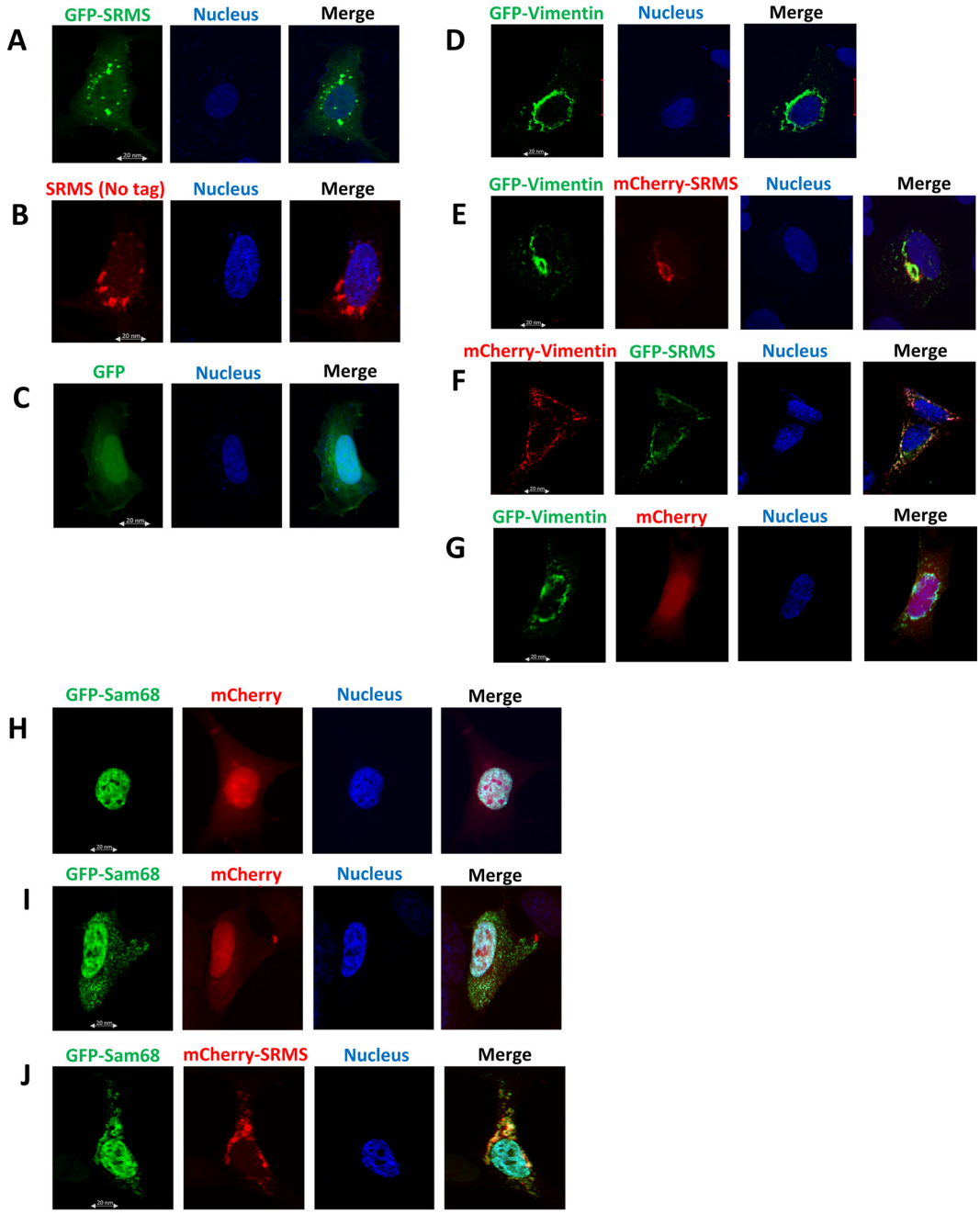

FIG. 9. **Co-localization of SRMS with vimentin and Sam68.** Vectors encoding: *A*, GFP-wild type SRMS, *B*, untagged wild type SRMS, or *C*, GFP alone were exogenously introduced in HEK293 cells. Transfected cells were fixed, permeabilized and ectopic untagged SRMS detected using primary SRMS antibodies and secondary anti-mouse Texas red antibodies. Nuclei were stained with DAPI. Images were acquired on a confocal microscope. *D*, HEK293 cells were transfected with a vector encoding GFP-vimentin alone or *E*, co-transfected with vectors encoding GFP-vimentin and mCherry-SRMS (wild type), *F*, mcherry-vimentin and GFP-wild type SRMS or *G*, GFP-vimentin and mcherry alone. Co-localization between both proteins was determined via confocal microscopy. *H* and *I*, HEK293 cells were co-transfected with either GFP-Sam68 and mcherry alone or *J*, GFP-Sam68 and mcherry-wild type SRMS. Co-localization between Sam68 and SRMS was determined via confocal microscopy. Scale bar, 20 nm.

either parental, scramble siRNA or SRMS siRNA-transfected cells. First, we observed a significant knockdown of endogenous SRMS in the SRMS siRNA-transfected cells (Fig. 10*A*, lower panel). However, immunoblotting the Sam68 immunoprecipitates with general phosphotyrosine antibodies revealed no significant difference in Sam68 tyrosine-phosphorylation between SRMS-knockdown and parental or scramble siRNA-transfected cells (Fig. 10*A*, top panel). This implied that under steady-state conditions endogenous SRMS has no impact on the tyrosine-phosphorylation of endogenous Sam68. Previous

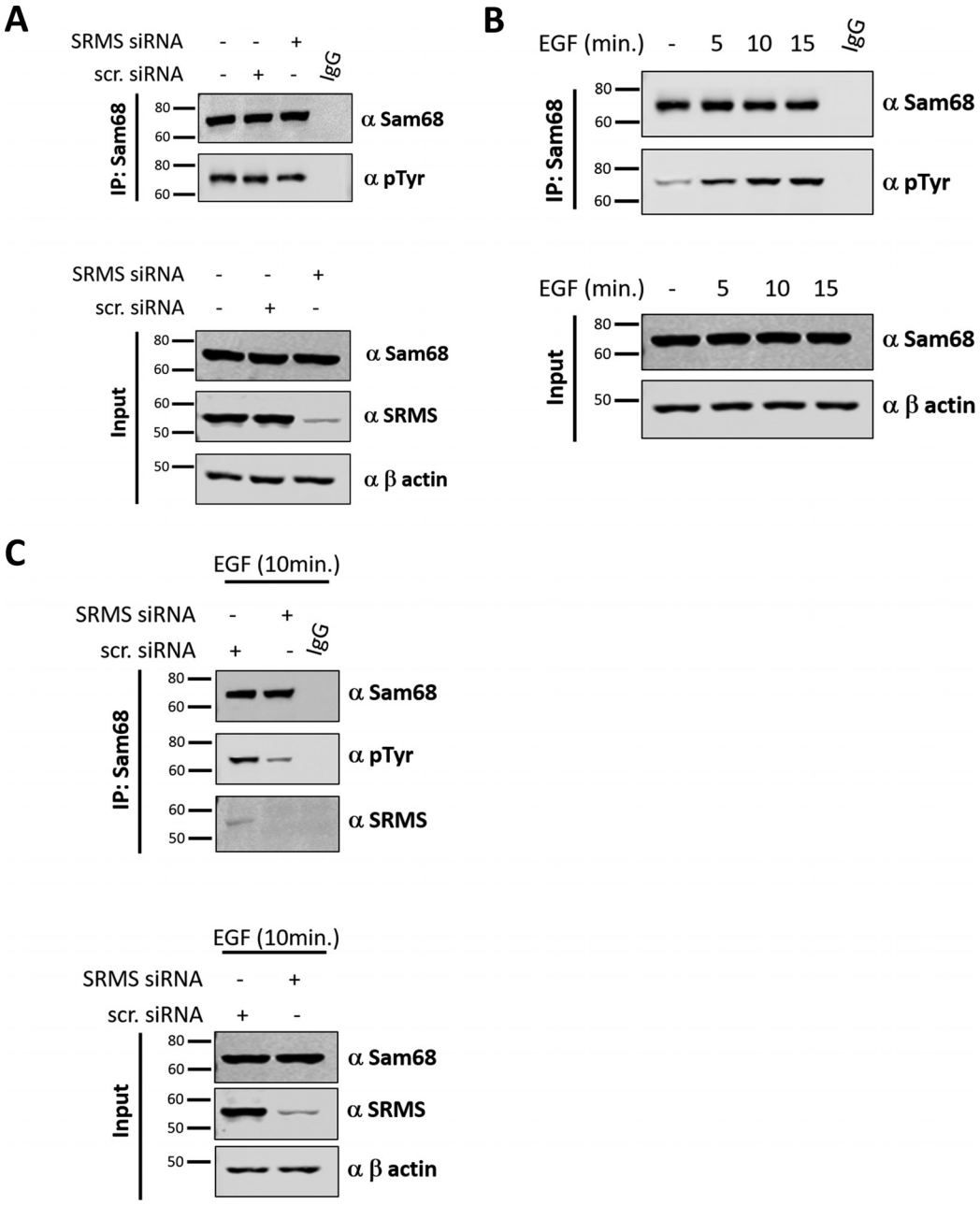

FIG. 10. **EGF-induced Sam68 phosphorylation mediated by SRMS.** *A*, MDA-MB 231 cells were transfected with either scramble siRNA or siRNA against SRMS. Parental and siRNA-transfected cells were lysed and Sam68 immunoprecipitated using Sam68 antibodies. The immunoprecipitates were probed with antibodies against Sam68 and general phosphotyrosines. Input from the corresponding lysates were probed with antibodies against SRMS and Sam68. β-actin served as a loading control. *B*, Serum-starved MDA-MB 231 cells were either treated with 100 ng/ml EGF for the indicated time-points or left untreated. Sam68 was immunoprecipitated from the lysates derived from the untreated and treated cells. The immunoprecipitates were probed with antibodies against Sam68 and general phosphotyrosines. Input from the corresponding lysates were probed with antibodies against Sam68 and β-actin. *C*, MDA-MB 231 cells, transfected with either scramble siRNA or SRMS siRNA, were stimulated with 100 ng/ml EGF for the indicated time point and lysed. Sam68 was immunoprecipitated from the lysates and the immunoprecipitates probed with antibodies against Sam68, phosphotyrosines and SRMS. Input from the corresponding lysates were probed with antibodies against Sam68, SRMS and β-actin.

studies have shown that Sam68 is a downstream target of the EGFR-signaling pathway where Sam68 undergoes significant tyrosine-phosphorylation on stimulation of cells with EGF (30). Additionally, BRK has been shown to modulate the EGF-stimulated tyrosine-phosphorylation of Sam68 (30). We therefore tested if SRMS affects Sam68-phosphorylation in response to EGF-stimulation. We first stimulated serum-starved MDA-MB 231 cells with EGF at intervals of 5 min for up to 15 min. We then

immunoprecipitated endogenous Sam68 from either serum-starved or EGF-stimulated cells and assessed the tyrosine-phosphorylation status of Sam68 via immunoblotting with phosphotyrosine antibodies. As expected, we found that EGF-stimulation led to increased tyrosine-phosphorylation of endogenous Sam68 which peaked at 10 min post-stimulation (Fig. 10*B*). Next, we stimulated control and SRMS-depleted MDA-MB 231 cells with EGF for 10 min and immunoprecipitated Sam68 to probe with phosphotyrosine antibodies. We found that knocking down endogenous SRMS led to reduced EGF-stimulated tyrosine-phosphorylation of Sam68 compared with scramble siRNA-transfected cells (Fig. 10*C*). Furthermore, upon increased exposure of the immunoblot we observed a faint but noticeable amount of SRMS coprecipitating with Sam68 implying that both proteins can associate in these cells (Fig. 10*C*). Our results therefore show that SRMS regulates the phosphorylation of Sam68 in an EGF-dependent manner in MDA-MB 231 cells. This furthermore underscores the potential physiological significance of Sam68 as a substrate of SRMS.

DISCUSSION

SRMS is a non-receptor tyrosine kinase of the BRK family kinases. Unlike BRK and FRK, SRMS remains a largely understudied member of the family. We previously characterized the enzymatic activity of SRMS and reported that wild type SRMS is enzymatically active and induces the tyrosine-phosphorylation of several proteins when exogenously expressed in mammalian cells (6). Ours represents the first quantitative phosphoproteomics study to identify a vast pool of novel candidate SRMS substrates from mammalian cells ectopically expressing the wild type SRMS kinase. Our unbiased analyses resulted in the identification of 1129 unique tyrosine-phosphorylated peptides in wild type SRMS-expressing cells. These were mapped to 663 unique proteins which were determined to be candidate SRMS substrates because the corresponding phosphopeptides were identified exclusively in cells expressing ectopic wild type SRMS. Importantly, we identified DOK1 as a hyperphosphorylated protein in SRMS-overexpressing cells. This confirmed our previous findings where we characterized DOK1 as a bona fide SRMS substrate and demonstrated that endogenous DOK1 was phosphorylated by ectopic SRMS in HEK293 cells. Furthermore, as expected, the peptide corresponding to SRMS Y380 was identified as one of the major phosphopeptides from our MS analyses (Table I). We also identified 14 novel tyrosine-phosphorylated sites in SRMS (Table I) which may either represent SRMS autophosphorylation sites or target sites for other tyrosine kinases. The biochemical and functional significance associated with these phospho-sites may be worth investigating in future studies. Intriguingly, we found 117 tyrosine-phosphorylated peptides in control cells but not in cells expressing ectopic SRMS (Fig. 4*B*). Notably, of the 663 identified tyrosine-phosphorylated proteins in SRMS-expressing cells, 6 are tyrosine-phosphatases (PTPRA, PTPRE, PTPN6, PTPN11, PTPRK, PTPN18). It is possible that SRMS-mediated tyrosine phosphorylation may either directly or indirectly regulate the tyrosine-phosphatase activity of one or several of these phosphatases potentially leading to the de-phosphorylation of specific targets. This may at least partly explain why the 117 tyrosine-phosphorylated peptides were identified in the control cells but not the SRMS-expressing cells.

It may be noted that similar earlier phosphoproteomics studies have identified candidate substrates from cells overexpressing specific kinases (23, 70–72). However, it can be argued that such approaches offer limited insights into the physiological context of kinase-substrate interactions. Native phosphorylation events occurring at the cellular level, either in the presence or absence of relevant biological stimuli, are a more appropriate representation of physiological kinase activities. To this end, alternative approaches involve the modulation of either the expression level or catalytic activity of native kinases to identify stoichiometric differences among phosphorylated proteins between the control and test conditions (24, 27, 70, 73). However, screening for physiological substrates of uncharacterized kinases can be particularly challenging. In the case of SRMS, the expression of the kinase has been detected in various breast cancer cell lines (6, 74). Other groups have reported the expression of SRMS in various murine organs (5, 12). However, the activation status of endogenous SRMS in these cells is not known. The phosphorylation of the activation loop tyrosine is a primary indicator of enzymatic activation in tyrosine kinases (15). Unlike c-Src (75) and BRK (76), no commercial antibodies exist to detect the phosphorylation of the SRMS activation-loop tyrosine residue (Y380). Additionally, whereas various specific chemical inhibitors of Src (77) and BRK (76) have been characterized, to our knowledge, no such specific inhibitors of SRMS enzymatic activity have been reported. Considering these technical shortcomings, we reasoned that the overexpression of the catalytically active wild type SRMS kinase in human cells may represent a reasonably viable alternative strategy to identify the cellular substrates of the kinase. Additionally, we have previously reported that both endogenous and ectopic SRMS localizes to cytoplasmic punctate structures. This implies that the localization and therefore the biochemical and cellular functions of ectopic SRMS may likely be similarly regulated. This further highlights the potential biological significance of the candidate substrates that were identified in our study.

Other groups have reported the identification of high-confidence kinase substrates via similar phosphoproteomics approaches by correlating the identified phospho-sites with known or well-characterized consensus substrate motifs of the kinase (25, 78, 79). Deng *et al.* identified *xIYx* and *YxxV* as two potential consensus substrate motifs of SRMS using an arrayed positional scanning peptide library (80). Our *in silico* analyses of the phospho-sites derived from candidate SRMS substrates uncovered various overrepresented motif patterns

(Fig. 5 and supplemental Fig. S3). Surprisingly, the *xIYx* and *YxxV* motifs were not among those identified in our analyses. It is not clear whether the motifs we identified in the present study were among the positional peptide variants tested by Deng *et al.* (80). Furthermore, though we identified *KxY* as one of the top candidate SRMS consensus motifs (Fig. 5 and supplemental Fig. S3 and S4), our validation analyses using peptide arrays revealed that the Vimentin Y383 peptide corresponding to the *RxY* motif displayed relatively increased phosphorylation compared with the other motifs (Table II and Fig. 7). It may be noted that various factors govern enzyme-substrate specificity in a cellular context. The sub-cellular localization as well as the intermolecular interactions between the kinase and substrate proteins represent key factors that contribute to the enzyme-substrate specificity (15). Additionally, when performed exclusively, *in vitro* studies involving peptide arrays may not accurately recapitulate physiologically relevant conditions favoring enzyme-substrate interactions. Moreover, the phosphorylation of a peptide is not entirely representative of the phosphorylation of the same sequence within a globular protein. All this may partly explain why our motif analyses of the candidate cellular SRMS substrates did not identify the two motifs described previously (80). We therefore reason that the identification of candidate kinase motifs from cell-based phosphoproteomics studies would likely provide rational opportunities for motif-validation in *in vitro* studies, such as with peptide arrays.

Our analyses using peptide arrays revealed that the phosphorylation of several peptides could not be validated because these were rendered statistically insignificant. Importantly, it has been noted that because of technical reasons data normalization measures tend to account for the loss of information from nearly 50% to 70% of peptides printed on such arrays (58). Therefore, we normally use quasi-stringent t-testing (p value < 0.1) in our analyses to limit the bias associated with stringent statistical thresholds (81, 82). This method of applying a quasi-stringent t-testing threshold in peptide array analyses has also been described by Scholma *et al.* (58).

Using the g:Profiler platform (41), we identified various biological processes/pathways enriched by the candidate SRMS substrates (Fig. 6*A* and 6*B*). RNA processing emerged as one of the major functional clusters associated with the candidate SRMS substrates (Fig. 6*A* and 6*B*). Sam68 was one of the proteins annotated in this cluster (supplemental Table S5). Sam68 is a KH domain-containing RNA-binding protein (RBP) shown to regulate several processes including pre-mRNA splicing, mRNA translation, nuclear export, RNA stability, signal transduction, and cell cycle progression (30, 83). Despite its predominantly nuclear localization, Sam68 is a major substrate of Src in the cytoplasm during mitosis (84), and of BRK in the nucleus (30). Both, the subcellular localization Sam68 and its RNA-binding functions are modulated by phosphorylation (30, 83). Other tyrosine kinases known to target Sam68 include Fyn, Lck, Tec, Jak3, BRK, Zap70, Btk or the insulin receptor (30, 85, 86). We validated Sam68 as a bona fide SRMS substrate via coimmunoprecipitation analyses and direct *in vitro* analyses (Fig. 8*C*, 8*D*, and 8*E*). We furthermore demonstrated that Sam68 displays a partial cytoplasmic localization (Fig. 9*I*) and that cytoplasmic Sam68 colocalizes with SRMS *in vivo* (Fig. 9*J*). More importantly, we determined that SRMS plays an important role in the EGF-induced tyrosine-phosphorylation of Sam68. In a previous study it was shown that BRK expression is also needed for the efficient phosphorylation of Sam68 upon EGF-stimulation. Specifically, the study demonstrated that Sam68-Y440 was a major site targeted by BRK *in vivo*. Our MS analysis identified Sam68-Y167 as a hyperphosphorylated site in cells expressing ectopic SRMS implying that Sam68-Y167 may potentially be a major SRMS target site. Taken together, because kinase functions are known to be tightly regulated in a temporal and spatial context, our results indicate that the biochemical and cellular functions of SRMS, with respect to Sam68, may be partly regulated under specific stimuli such as in response to EGF.

Vimentin was identified as one of the top candidate SRMS substrates in our phosphoproteomics analyses. We validated vimentin as a *bona fide* SRMS substrate via *in vitro* and *in vivo* assays and showed that both proteins colocalize in the cytoplasm (Fig. 8*A*, 8*B*, and 8*F*; Fig. 9*E* and 9*F*). Vimentin is the most common intermediate filament (IF) and an essential component of the cytoskeleton (87). Vimentin is post-translationally modified by a variety of kinases on both Tyr (88) and Ser/Thr residues (60) leading to the structural re-arrangements of vimentin IF filaments (89). To our knowledge, the phospho-sites we identified in vimentin in the present study have not been functionally characterized before and may warrant future studies. Through immunoprecipitation assays we examined whether the phosphorylation of Vimentin was regulated by endogenous SRMS in two different breast cancer cell lines, namely, the MDA-MB 231 and MCF7 cell lines (data not shown). Additionally, we treated the cells with EGF to see if, like Sam68, Vimentin phosphorylation is responsive to EGF-stimulation in these cell lines. However, we did not observe the tyrosine phosphorylation of endogenous Vimentin either under untreated or EGF-treated conditions in both cell lines (data not shown). This may imply that the tyrosine-phosphorylation of Vimentin is likely more tightly regulated in these cells and further studies would be required to characterize the physiological significance of Vimentin as a SRMS substrate.

A recent study by Potts *et al.* showed that knockdown of SRMS resulted in increased light chain 3 (LC3)-positive puncta per cell and decreased abundance of GFP-LC3 in an autophagy-related 5 (ATG5)–dependent manner (74). Overexpression of SRMS decreased the number of LC3-postive puncta per cell, suggesting that SRMS potentially inhibits autophagy upstream of autophagosome formation (74). However, in our study, functional gene enrichment analyses of these candidate substrates did not identify any autophagy-linked cellular process or pathway. Therefore, it is possible

that the regulation of autophagy by SRMS, as reported by Potts *et al.*, is not kinase-dependent or may likely be influenced in a tissue or cell line-specific context. It is possible that examining the SRMS-interacting partners may reveal proteins that are linked to autophagy.

In the present study we used ectopic SRMS to identify the candidate SRMS cellular substrates. A few or several of these substrates are likely to represent physiologically important substrates of SRMS. This will certainly lead to a better understanding of the biochemical and functional specificity associated with SRMS in a physiological context. In conclusion, our phosphoproteomics analyses helped uncover a vast array of novel candidate SRMS substrates which provides insights into the biochemical substrate motif specificities and the potentially diverse cellular roles played by the tyrosine kinase. Given that SRMS is the least studied member of the BRK family kinases, our findings provide an important resource for future mechanistic studies to investigate the cellular and physiological functions of the kinase.

Acknowledgments—We thank Dr. Charles Farnsworth (CST) for his invaluable input and Jennifer Chung (SCBT) for her resourceful contributions to the present study. We would also like to express our gratitude to Dr. William (Bill) Roesler, Department of Biochemistry, University of Saskatchewan for providing insightful comments and feedback on the manuscript.

DATA AVAILABILITY

The mass spectrometry proteomics data (including the files for viewing the annotated spectra) have been deposited to the ProteomeXchange Consortium (38) via the PRIDE (39) partner repository with the dataset identifier PXD006809. The data is publically available and can be accessed through the following weblink: http://www.ebi.ac.uk/pride/archive/projects/PXD006809.

* This work has been supported by the NSERC President's fund administered by the University of Saskatchewan and the NSERC Discovery grant (RGPIN-2017-05564).

S This article contains supplemental material.

** To whom correspondence should be addressed: Department of Biochemistry, College of Medicine, University of Saskatchewan, 107 Wiggins Road, Saskatoon, SK. S7N 5E5, Canada. Tel.: 306-966-4586; Fax: 306-966-4390; E-mail: Kiven.lukong@usuask.ca.

REFERENCES

1. Robinson, D. R., Wu, Y. M., and Lin, S. F. (2000) The protein tyrosine kinase family of the human genome. *Oncogene* **19,** 5548–5557
2. Manning, G., Whyte, D. B., Martinez, R., Hunter, T., and Sudarsanam, S. (2002) The protein kinase complement of the human genome. *Science* **298,** 1912–1934
3. Goel, R. K., and Lukong, K. E. (2015) Tracing the footprints of the breast cancer oncogene BRK - Past till present. *Biochim. Biophys. Acta* **1856,** 39–54
4. Goel, R. K., and Lukong, K. E. (2016) Understanding the cellular roles of Fyn-related kinase (FRK): implications in cancer biology. *Cancer Metastasis Rev.* **35,** 179–199
5. Kohmura, N., Yagi, T., Tomooka, Y., Oyanagi, M., Kominami, R., Takeda, N., Chiba, J., Ikawa, Y., and Aizawa, S. (1994) A novel nonreceptor tyrosine kinase, Srm: cloning and targeted disruption. *Mol. Cell. Biol.* **14,** 6915–6925
6. Goel, R. K., Miah, S., Black, K., Kalra, N., Dai, C., and Lukong, K. E. (2013) The unique N-terminal region of SRMS regulates enzymatic activity and phosphorylation of its novel substrate docking protein 1. *FEBS J.* **280,** 4539–4559
7. Pawson, T. (1994) SH2 and SH3 domains in signal transduction. *Adv. Cancer Res.* **64,** 87–110
8. Pawson, T., Olivier, P., Rozakis-Adcock, M., McGlade, J., and Henkemeyer, M. (1993) Proteins with SH2 and SH3 domains couple receptor tyrosine kinases to intracellular signalling pathways. *Philosophical Trans. Roy. Soc. London.* **340,** 279–285
9. Pawson, T., and Gish, G. D. (1992) SH2 and SH3 domains: from structure to function. *Cell* **71,** 359–362
10. Koch, C. A., Anderson, D., Moran, M. F., Ellis, C., and Pawson, T. (1991) SH2 and SH3 domains: elements that control interactions of cytoplasmic signaling proteins. *Science* **252,** 668–674
11. Fan, G., Aleem, S., Yang, M., Miller, W. T., and Tonks, N. K. (2015) Protein-tyrosine phosphatase and kinase specificity in regulation of SRC and breast tumor kinase. *J. Biol. Chem.* **290,** 15934–15947
12. Kawachi, Y., Nakauchi, H., and Otsuka, F. (1997) Isolation of a cDNA encoding a tyrosine kinase expressed in murine skin. *Exp. Dermatol.* **6,** 140–146
13. Casaletto, J. B., and McClatchey, A. I. (2012) Spatial regulation of receptor tyrosine kinases in development and cancer. *Nat. Rev. Cancer* **12,** 387–400
14. Nurmio, M., Joki, H., Kallio, J., Maatta, J. A., Vaananen, H. K., Toppari, J., Jahnukainen, K., and Laitala-Leinonen, T. (2011) Receptor tyrosine kinase inhibition causes simultaneous bone loss and excess bone formation within growing bone in rats. *Toxicol. Appl. Pharmacol.* **254,** 267–279
15. Hunter, T. (2009) Tyrosine phosphorylation: thirty years and counting. *Curr. Opinion Cell Biol.* **21,** 140–146
16. Nolen, B., Taylor, S., and Ghosh, G. (2004) Regulation of protein kinases; controlling activity through activation segment conformation. *Mol. Cell* **15,** 661–675
17. Hubbard, S. R., Mohammadi, M., and Schlessinger, J. (1998) Autoregulatory mechanisms in protein-tyrosine kinases. *J. Biol. Chem.* **273,** 11987–11990
18. Hubbard, S. R. (2002) Protein tyrosine kinases: autoregulation and small-molecule inhibition. *Curr. Opinion Structural Biol.* **12,** 735–741
19. Ubersax, J. A., and Ferrell, J. E., Jr. (2007) Mechanisms of specificity in protein phosphorylation. *Nat. Rev. Mol. Cell Biol.* **8,** 530–541
20. Mok, J., Kim, P. M., Lam, H. Y., Piccirillo, S., Zhou, X., Jeschke, G. R., Sheridan, D. L., Parker, S. A., Desai, V., Jwa, M., Cameroni, E., Niu, H., Good, M., Remenyi, A., Ma, J. L., Sheu, Y. J., Sassi, H. E., Sopko, R., Chan, C. S., De Virgilio, C., Hollingsworth, N. M., Lim, W. A., Stern, D. F., Stillman, B., Andrews, B. J., Gerstein, M. B., Snyder, M., and Turk, B. E. (2010) Deciphering protein kinase specificity through large-scale analysis of yeast phosphorylation site motifs. *Sci. Signal.* **3,** ra12
21. Amanchy, R., Kandasamy, K., Mathivanan, S., Periaswamy, B., Reddy, R., Yoon, W. H., Joore, J., Beer, M. A., Cope, L., and Pandey, A. (2011) Identification of Novel Phosphorylation Motifs Through an Integrative Computational and Experimental Analysis of the Human Phosphoproteome. *J. Proteomics Bioinformatics* **4,** 22–35
22. Xue, L., Geahlen, R. L., and Tao, W. A. (2013) Identification of direct tyrosine kinase substrates based on protein kinase assay-linked phosphoproteomics. *Mol. Cell. Proteomics* **12,** 2969–2980
23. Amanchy, R., Zhong, J., Molina, H., Chaerkady, R., Iwahori, A., Kalume, D. E., Gronborg, M., Joore, J., Cope, L., and Pandey, A. (2008) Identification of c-Src tyrosine kinase substrates using mass spectrometry and peptide microarrays. *J. Proteome Res.* **7,** 3900–3910
24. Amanchy, R., Zhong, J., Hong, R., Kim, J. H., Gucek, M., Cole, R. N., Molina, H., and Pandey, A. (2009) Identification of c-Src tyrosine kinase substrates in platelet-derived growth factor receptor signaling. *Mol. Oncol.* **3,** 439–450
25. Courcelles, M., Fremin, C., Voisin, L., Lemieux, S., Meloche, S., and Thibault, P. (2013) Phosphoproteome dynamics reveal novel ERK1/2 MAP kinase substrates with broad spectrum of functions. *Mol. Systems Biol.* **9,** 669
26. Bian, Y., Ye, M., Wang, C., Cheng, K., Song, C., Dong, M., Pan, Y., Qin, H., and Zou, H. (2013) Global screening of CK2 kinase substrates by an integrated phosphoproteomics workflow. *Sci. Reports* **3,** 3460
27. Hsu, P. P., Kang, S. A., Rameseder, J., Zhang, Y., Ottina, K. A., Lim, D., Peterson, T. R., Choi, Y., Gray, N. S., Yaffe, M. B., Marto, J. A., and

Sabatini, D. M. (2011) The mTOR-regulated phosphoproteome reveals a mechanism of mTORC1-mediated inhibition of growth factor signaling. *Science* **332,** 1317–1322
28. Larance, M., and Lamond, A. I. (2015) Multidimensional proteomics for cell biology. *Nature reviews. Mol. Cell Biol.* **16,** 269–280
29. Roux, P. P., and Thibault, P. (2013) The coming of age of phosphoproteomics–from large data sets to inference of protein functions. *Mol. Cell. Proteomics* **12,** 3453–3464
30. Lukong, K. E., Larocque, D., Tyner, A. L., and Richard, S. (2005) Tyrosine phosphorylation of sam68 by breast tumor kinase regulates intranuclear localization and cell cycle progression. *J. Biol. Chem.* **280,** 38639–38647
31. Chen, T., Boisvert, F. M., Bazett-Jones, D. P., and Richard, S. (1999) A role for the GSG domain in localizing Sam68 to novel nuclear structures in cancer cell lines. *Mol. Biol. Cell* **10,** 3015–3033
32. Elias, J. E., and Gygi, S. P. (2007) Target-decoy search strategy for increased confidence in large-scale protein identifications by mass spectrometry. *Nat. Methods* **4,** 207–214
33. Cox, J., and Mann, M. (2008) MaxQuant enables high peptide identification rates, individualized p.p.b.-range mass accuracies and proteome-wide protein quantification. *Nat. Biotechnol.* **26,** 1367–1372
34. Sharma, K., D'Souza, R. C., Tyanova, S., Schaab, C., Wisniewski, J. R., Cox, J., and Mann, M. (2014) Ultradeep human phosphoproteome reveals a distinct regulatory nature of Tyr and Ser/Thr-based signaling. *Cell Rep.* **8,** 1583–1594
35. Tyanova, S., Temu, T., and Cox, J. (2016) The MaxQuant computational platform for mass spectrometry-based shotgun proteomics. *Nat. Protoc.* **11,** 2301–2319
36. Mertins, P., Udeshi, N. D., Clauser, K. R., Mani, D. R., Patel, J., Ong, S. E., Jaffe, J. D., and Carr, S. A. (2012) iTRAQ labeling is superior to mTRAQ for quantitative global proteomics and phosphoproteomics. *Mol. Cell. Proteomics* **11,** M111.014423
37. Grimes, M. L., Lee, W. J., van der Maaten, L., and Shannon, P. (2013) Wrangling phosphoproteomic data to elucidate cancer signaling pathways. *PLoS ONE* **8,** e52884
38. Vizcaino, J. A., Deutsch, E. W., Wang, R., Csordas, A., Reisinger, F., Rios, D., Dianes, J. A., Sun, Z., Farrah, T., Bandeira, N., Binz, P. A., Xenarios, I., Eisenacher, M., Mayer, G., Gatto, L., Campos, A., Chalkley, R. J., Kraus, H. J., Albar, J. P., Martinez-Bartolome, S., Apweiler, R., Omenn, G. S., Martens, L., Jones, A. R., and Hermjakob, H. (2014) ProteomeXchange provides globally coordinated proteomics data submission and dissemination. *Nat. Biotechnol.* **32,** 223–226
39. Vizcaino, J. A., Csordas, A., del-Toro, N., Dianes, J. A., Griss, J., Lavidas, I., Mayer, G., Perez-Riverol, Y., Reisinger, F., Ternent, T., Xu, Q. W., Wang, R., and Hermjakob, H. (2016) 2016 update of the PRIDE database and its related tools. *Nucleic Acids Res.* **44,** D447–D456
40. Trost, B., Kindrachuk, J., Maattanen, P., Napper, S., and Kusalik, A. (2013) PIIKA 2: an expanded, web-based platform for analysis of kinome microarray data. *PloS One* **8,** e80837
41. Reimand, J., Arak, T., Adler, P., Kolberg, L., Reisberg, S., Peterson, H., and Vilo, J. (2016) g:Profiler-a web server for functional interpretation of gene lists (2016 update). *Nucleic Acids Res.* **44,** W83–W89
42. Hornbeck, P. V., Zhang, B., Murray, B., Kornhauser, J. M., Latham, V., and Skrzypek, E. (2015) PhosphoSitePlus, 2014: mutations, PTMs and recalibrations. *Nucleic Acids Res.* **43,** D512–D520
43. Merico, D., Isserlin, R., Stueker, O., Emili, A., and Bader, G. D. (2010) Enrichment map: a network-based method for gene-set enrichment visualization and interpretation. *PLoS One* **5,** e13984
44. Schlessinger, J., and Lemmon, M. A. (2003) SH2 and PTB domains in tyrosine kinase signaling. *Science's STKE* **2003,** RE12
45. Kavanaugh, W. M., Turck, C. W., and Williams, L. T. (1995) PTB domain binding to signaling proteins through a sequence motif containing phosphotyrosine. *Science* **268,** 1177–1179
46. Yaffe, M. B. (2002) Phosphotyrosine-binding domains in signal transduction. *Nature reviews. Mol. Cell Biol.* **3,** 177–186
47. Cox, J., Neuhauser, N., Michalski, A., Scheltema, R. A., Olsen, J. V., and Mann, M. (2011) Andromeda: a peptide search engine integrated into the MaxQuant environment. *J Proteome Res.* **10,** 1794–1805
48. Tyanova, S., Temu, T., Sinitcyn, P., Carlson, A., Hein, M. Y., Geiger, T., Mann, M., and Cox, J. (2016) The Perseus computational platform for comprehensive analysis of (prote)omics data. *Nat. Methods* **13,** 731–740
49. Conrads, T. P., and Veenstra, T. D. (2005) An enriched look at tyrosine phosphorylation. *Nat. Biotechnol.* **23,** 36–37
50. Hunter, T. (1998) The Croonian Lecture 1997. The phosphorylation of proteins on tyrosine: its role in cell growth and disease. *Phil. Trans. Roy. Soc. London. Series B, Biological sciences* **353,** 583–605
51. Wang, T., Kettenbach, A. N., Gerber, S. A., and Bailey-Kellogg, C. (2012) MMFPh: a maximal motif finder for phosphoproteomics datasets. *Bioinformatics* **28,** 1562–1570
52. Chou, M. F., and Schwartz, D. (2011) Biological sequence motif discovery using motif-x. *Current Protocols Bioinformatics* Chapter 13, Unit 13 15–24
53. Amanchy, R., Periaswamy, B., Mathivanan, S., Reddy, R., Tattikota, S. G., and Pandey, A. (2007) A curated compendium of phosphorylation motifs. *Nat. Biotechnol.* **25,** 285–286
54. Parikh, K., Diks, S. H., Tuynman, J. H., Verhaar, A., Lowenberg, M., Hommes, D. W., Joore, J., Pandey, A., and Peppelenbosch, M. P. (2009) Comparison of peptide array substrate phosphorylation of c-Raf and mitogen activated protein kinase kinase kinase 8. *PloS One* **4,** e6440
55. Leung, G. C., Ho, C. S., Blasutig, I. M., Murphy, J. M., and Sicheri, F. (2007) Determination of the Plk4/Sak consensus phosphorylation motif using peptide spots arrays. *FEBS Lett.* **581,** 77–83
56. Diks, S. H., Kok, K., O'Toole, T., Hommes, D. W., van Dijken, P., Joore, J., and Peppelenbosch, M. P. (2004) Kinome profiling for studying lipopolysaccharide signal transduction in human peripheral blood mononuclear cells. *J. Biol. Chem.* **279,** 49206–49213
57. Wei, Y., Zou, Z., Becker, N., Anderson, M., Sumpter, R., Xiao, G., Kinch, L., Koduru, P., Christudass, C. S., Veltri, R. W., Grishin, N. V., Peyton, M., Minna, J., Bhagat, G., and Levine, B. (2013) EGFR-mediated Beclin 1 phosphorylation in autophagy suppression, tumor progression, and tumor chemoresistance. *Cell* **154,** 1269–1284
58. Scholma, J., Fuhler, G. M., Joore, J., Hulsman, M., Schivo, S., List, A. F., Reinders, M. J., Peppelenbosch, M. P., and Post, J. N. (2016) Improved intra-array and interarray normalization of peptide microarray phosphorylation for phosphorylome and kinome profiling by rational selection of relevant spots. *Sci. Reports* **6,** 26695
59. Ferrando, I. M., Chaerkady, R., Zhong, J., Molina, H., Jacob, H. K., Herbst-Robinson, K., Dancy, B. M., Katju, V., Bose, R., Zhang, J., Pandey, A., and Cole, P. A. (2012) Identification of targets of c-Src tyrosine kinase by chemical complementation and phosphoproteomics. *Mol. Cell. Proteomics* **11,** 355–369
60. Eriksson, J. E., He, T., Trejo-Skalli, A. V., Harmala-Brasken, A. S., Hellman, J., Chou, Y. H., and Goldman, R. D. (2004) Specific in vivo phosphorylation sites determine the assembly dynamics of vimentin intermediate filaments. *J. Cell Sci.* **117,** 919–932
61. Cheng, T. J., Tseng, Y. F., Chang, W. M., Chang, M. D., and Lai, Y. K. (2003) Retaining of the assembly capability of vimentin phosphorylated by mitogen-activated protein kinase-activated protein kinase-2. *J. Cell. Biochem.* **89,** 589–602
62. Feracci, M., Foot, J. N., Grellscheid, S. N., Danilenko, M., Stehle, R., Gonchar, O., Kang, H. S., Dalgliesh, C., Meyer, N. H., Liu, Y., Lahat, A., Sattler, M., Eperon, I. C., Elliott, D. J., and Dominguez, C. (2016) Structural basis of RNA recognition and dimerization by the STAR proteins T-STAR and Sam68. *Nat. Commun.* **7,** 10355
63. Mendez, M. G., Kojima, S., and Goldman, R. D. (2010) Vimentin induces changes in cell shape, motility, and adhesion during the epithelial to mesenchymal transition. *FASEB J.* **24,** 1838–1851
64. Flynn, M. P., Fiedler, S. E., Karlsson, A. B., Carr, D. W., Maizels, E. T., and Hunzicker-Dunn, M. (2016) Dephosphorylation of MAP2D enhances its binding to vimentin in preovulatory ovarian granulosa cells. *J. Cell Sci.* **129,** 2983–2996
65. Wrighton, K. H. (2016) Nuclear organization: Building nuclear bodies with RNA. *Nature Rev. Mol. Cell Biol.* **17,** 463
66. Huot, M. E., Brown, C. M., Lamarche-Vane, N., and Richard, S. (2009) An adaptor role for cytoplasmic Sam68 in modulating Src activity during cell polarization. *Mol. Cell. Biol.* **29,** 1933–1943
67. Paronetto, M. P., Zalfa, F., Botti, F., Geremia, R., Bagni, C., and Sette, C. (2006) The nuclear RNA-binding protein Sam68 translocates to the cytoplasm and associates with the polysomes in mouse spermatocytes. *Mol. Biol. Cell* **17,** 14–24
68. Liao, W. T., Liu, J. L., Wang, Z. G., Cui, Y. M., Shi, L., Li, T. T., Zhao, X. H., Chen, X. T., Ding, Y. Q., and Song, L. B. (2013) High expression level and

nuclear localization of Sam68 are associated with progression and poor prognosis in colorectal cancer. *BMC Gastroenterol.* **13,** 126
69. Richard, S. (2010) Reaching for the stars: Linking RNA binding proteins to diseases. *Adv. Exp. Med. Biol.* **693,** 142–157
70. Xue, L., Wang, W. H., Iliuk, A., Hu, L., Galan, J. A., Yu, S., Hans, M., Geahlen, R. L., and Tao, W. A. (2012) Sensitive kinase assay linked with phosphoproteomics for identifying direct kinase substrates. *Proc. Natl. Acad. Sci. U.S.A.* **109,** 5615–5620
71. Wu, F., Wang, P., Zhang, J., Young, L. C., Lai, R., and Li, L. (2010) Studies of phosphoproteomic changes induced by nucleophosmin-anaplastic lymphoma kinase (ALK) highlight deregulation of tumor necrosis factor (TNF)/Fas/TNF-related apoptosis-induced ligand signaling pathway in ALK-positive anaplastic large cell lymphoma. *Mol. Cell. Proteomics* **9,** 1616–1632
72. Leroy, C., Fialin, C., Sirvent, A., Simon, V., Urbach, S., Poncet, J., Robert, B., Jouin, P., and Roche, S. (2009) Quantitative phosphoproteomics reveals a cluster of tyrosine kinases that mediates SRC invasive activity in advanced colon carcinoma cells. *Cancer Res.* **69,** 2279–2286
73. Poss, Z. C., Ebmeier, C. C., Odell, A. T., Tangpeerachaikul, A., Lee, T., Pelish, H. E., Shair, M. D., Dowell, R. D., Old, W. M., and Taatjes, D. J. (2016) Identification of mediator kinase substrates in human cells using cortistatin A and quantitative phosphoproteomics. *Cell Reports* **15,** 436–450
74. Potts, M. B., Kim, H. S., Fisher, K. W., Hu, Y., Carrasco, Y. P., Bulut, G. B., Ou, Y. H., Herrera-Herrera, M. L., Cubillos, F., Mendiratta, S., Xiao, G., Hofree, M., Ideker, T., Xie, Y., Huang, L. J., Lewis, R. E., MacMillan, J. B., and White, M. A. (2013) Using functional signature ontology (FUSION) to identify mechanisms of action for natural products. *Sci. Signaling* 6, ra90
75. Dong, L., Yu, W. M., Zheng, H., Loh, M. L., Bunting, S. T., Pauly, M., Huang, G., Zhou, M., Broxmeyer, H. E., Scadden, D. T., and Qu, C. K. (2016) Leukaemogenic effects of Ptpn11 activating mutations in the stem cell microenvironment. *Nature* **539,** 304–308
76. Jiang, J., Gui, F., He, Z., Li, L., Li, Y., Li, S., Wu, X., Deng, Z., Sun, X., Huang, X., Huang, W., Han, S., Zhang, T., Wang, Z., Jiao, B., Song, S., Wang, H., Chen, L., Zhou, D., Liu, Q., Ren, R., Zhang, J., and Deng, X. (2017) Targeting BRK-Positive Breast Cancers with Small-Molecule Kinase Inhibitors. *Cancer Res.* **77,** 175–186
77. Yeatman, T. J. (2004) A renaissance for SRC. *Nat. Rev. Cancer* **4,** 470–480
78. Francavilla, C., Lupia, M., Tsafou, K., Villa, A., Kowalczyk, K., Rakownikow Jersie-Christensen, R., Bertalot, G., Confalonieri, S., Brunak, S., Jensen, L. J., Cavallaro, U., and Olsen, J. V. (2017) Phosphoproteomics of Primary Cells Reveals Druggable Kinase Signatures in Ovarian Cancer. *Cell Reports* **18,** 3242–3256
79. Kettenbach, A. N., Schweppe, D. K., Faherty, B. K., Pechenick, D., Pletnev, A. A., and Gerber, S. A. (2011) Quantitative phosphoproteomics identifies substrates and functional modules of Aurora and Polo-like kinase activities in mitotic cells. *Sci. Signaling* **4,** rs5
80. Deng, Y., Alicea-Velazquez, N. L., Bannwarth, L., Lehtonen, S. I., Boggon, T. J., Cheng, H. C., Hytonen, V. P., and Turk, B. E. (2014) Global analysis of human nonreceptor tyrosine kinase specificity using high-density peptide microarrays. *J. Proteome Res.* **13,** 4339–4346
81. Napper, S., Dadgar, S., Arsenault, R. J., Trost, B., Scruten, E., Kusalik, A., and Shand, P. (2015) Induction of tissue- and stressor-specific kinomic responses in chickens exposed to hot and cold stresses. *Poultry Sci.* **94,** 1333–1345
82. Kindrachuk, J., Arsenault, R., Kusalik, A., Kindrachuk, K. N., Trost, B., Napper, S., Jahrling, P. B., and Blaney, J. E. (2012) Systems kinomics demonstrates Congo Basin monkeypox virus infection selectively modulates host cell signaling responses as compared to West African monkeypox virus. *Mol. Cell. Proteomics* **11,** M111.015701
83. Lukong, K. E., and Richard, S. (2003) Sam68, the KH domain-containing superSTAR. *Biochim. Biophys. Acta* **1653,** 73–86
84. Taylor, S. J., Anafi, M., Pawson, T., and Shalloway, D. (1995) Functional interaction between c-Src and its mitotic target, Sam 68. *J. Biol. Chem.* **270,** 10120–10124
85. Di Fruscio, M., Chen, T., and Richard, S. (1999) Characterization of Sam68-like mammalian proteins SLM-1 and SLM-2: SLM-1 is a Src substrate during mitosis. *Proc. Natl. Acad. Sci. U.S.A.* **96,** 2710–2715
86. Sanchez-Jimenez, F., and Sanchez-Margalet, V. (2013) Role of Sam68 in post-transcriptional gene regulation. *Int. J. Mol. Sci.* **14,** 23402–23419
87. Jiu, Y., Peranen, J., Schaible, N., Cheng, F., Eriksson, J. E., Krishnan, R., and Lappalainen, P. (2017) Vimentin intermediate filaments control actin stress fiber assembly through GEF-H1 and RhoA. *J. Cell Sci.* **130,** 892–902
88. Chen, Y., Choong, L. Y., Lin, Q., Philp, R., Wong, C. H., Ang, B. K., Tan, Y. L., Loh, M. C., Hew, C. L., Shah, N., Druker, B. J., Chong, P. K., and Lim, Y. P. (2007) Differential expression of novel tyrosine kinase substrates during breast cancer development. *Mol. Cell. Proteomics* **6,** 2072–2087
89. Hyder, C. L., Pallari, H. M., Kochin, V., and Eriksson, J. E. (2008) Providing cellular signposts–post-translational modifications of intermediate filaments. *FEBS Lett.* **582,** 2140–2148